The BLIMP1 – EZH2 nexus in a non-Hodgkin lymphoma

Kimberley Jade Anderson[1,2,6], Árný Björg Ósvaldsdóttir[1,2,6], Birgit Atzinger[1,2,6], Gunnhildur Ásta Traustadóttir[1,6], Kirstine Nolling Jensen[3,4,6], Aðalheiður Elín Lárusdóttir[1,2,6], Jón Þór Bergþorsson[2,5,6], Ingibjörg Harðardóttir[3,4,6], Erna Magnúsdóttir[1,2,6]

1. Department of Anatomy, Faculty of Medicine, Vatnsmýrarvegur 16, 101 Reykjavik, Iceland
2. Department of Biomedical Science, Faculty of Medicine, 101 Reykjavík, Iceland
3. Department of Biochemistry and Molecular Biology, Faculty of Medicine, 101 Reykjavík, Iceland
4. Department of Immunology, Landspitali-The National University Hospital of Iceland, 101 Reykjavik, Iceland
5. Department of Laboratory Haematology, Landspitali-The National University Hospital of Iceland, 101 Reykjavik, Iceland
6. The University of Iceland Biomedical Center, Vatnsmýrarvegur 16, 101 Reykjavík Iceland

Abstract

Waldenström's macroglobulinemia (WM) is a non-hodgkin lymphoma, affecting antibody-secreting lymphoplasmacytic cells in the bone marrow. BLIMP1 is a key transcriptional repressor which drives the transition from B cells to plasma cells and is essential for antibody secretion. Despite this, a potential role for BLIMP1 in WM has not yet been explored. Here we provide evidence of a crucial role for BLIMP1 in the survival of WM cells. We further demonstrate that BLIMP1 is necessary for the expression of the histone methyltransferase EZH2 in both WM and multiple myeloma, most likely through a regulation of proteasomal targeting of EZH2. Chromatin immunoprecipitation analysis and genome wide transcriptome profiling show that the two factors co-operate in regulating genes involved in cancer cell immune evasion. Co-cultures of natural killer cells and WM cells further reveal that both factors participate directly in immune evasion, promoting escape from natural killer cell mediated cytotoxicity. Together, the interplay of BLIMP1 and EZH2 plays a vital role in promoting the survival of WM cells.

Introduction

Waldenström's macroglobulinemia (WM) is a disease characterised by the expansion of monoclonal lymphoplasmacytic cells in the bone marrow, which secrete immunoglobulin M (IgM) (Vijay & Gertz, 2007). Around 3-6 people per million are diagnosed with WM every year, although this varies by geographical region (Brandefors, Melin et al., 2018, Iwanaga, Chiang et al., 2014, Kyle, Larson et al., 2018, Wang, Chen et al., 2012). The activating mutation, $MYD88^{L265P}$, is present in ~96% of untreated patients and serves as a key oncogenic driver of WM, as well as in a subset of activated B cell-like diffuse large B cell lymphoma (ABC-DLBCL) (Treon, Xu et al., 2012, Xu, Hunter et al., 2014, Yu, Li et al., 2018).

The transcription factor B-lymphocyte induced maturation protein-1 (BLIMP1) is a master regulator of terminal B-cell development, and acts via recruitment of co-factors to chromatin (Győry, Wu et al., 2004, Ren, Chee et al., 1999, Yu, Angelin-Duclos et al., 2000). BLIMP1 also has essential functions in the

development of many cells and tissues, including primordial germ cells (Ohinata, Payer et al., 2005), the epidermis (Magnúsdóttir, Kalachikov et al., 2007), and the placenta (Vincent, Dunn et al., 2005), to name a few. Interestingly, BLIMP1 is known to be induced downstream of toll like receptor engagement (Morgan, Magnusdottir et al., 2009). Furthermore, LPS-stimulated B cells from MYD88 knock-out mice show decreased expression levels of *Prdm1*, the gene encoding BLIMP1, showing that BLIMP1 is induced downstream of MYD88 (Pasare & Medzhitov, 2005). BLIMP1 was described early on as a repressor of immune signalling mechanisms in B cells, including the Class II transactivator (*CIITA*) (Piskurich, Lin et al., 2000b, Tooze, Stephenson et al., 2006), B cell receptor signalling, and surface antigens and receptors (Shaffer, Lin et al., 2002). It is a key regulator of plasma cell terminal differentiation and antibody secretion (Minnich, Tagoh et al., 2016, Shaffer et al., 2002, Tellier, Shi et al., 2016) and is necessary for the survival of multiple myeloma cells (Lin, Kuo et al., 2007). Conversely, BLIMP1 is frequently inactivated in DLBCL, and is thought to function as a tumour suppressor in that context, consistent with its role in repressing cell cycle genes during the transition from mature B-cells to plasma cells (Calado, Zhang et al., 2010, Mandelbaum, Bhagat et al., 2010, Pasqualucci, Compagno et al., 2006, Shaffer et al., 2002). Furthermore, in WM, there are frequent heterozygous losses of *PRDM1* (Schop, Kuehl et al., 2002), however despite this, BLIMP1 is expressed in a subset of WM lymphoplasmacytic cells (Roberts, Chadburn et al., 2013, Zhou, Liu et al., 2014), consistent with the requirement for BLIMP1 in antibody secretion (Minnich et al., 2016, Savitsky & Calame, 2006, Shapiro-Shelef, Lin et al., 2003). Given the contradictory roles of BLIMP1 in ABC-DLBCL and myeloma, its involvement in WM has been critically under studied.

Another important player in plasma cell differentiation, EZH2 has been described as both a physical and genetic interaction partner of BLIMP1 (Guo, Price et al., 2018, Minnich et al., 2016). The interaction was first suggested in mouse primordial germ cells (PGCs), where BLIMP1 and EZH2 were found to bind to the same sites on a genome-wide scale (Kurimoto, Yabuta et al., 2015, Magnúsdóttir, Dietmann et al., 2013). EZH2 functions as the catalytic component of the polycomb repressive complex 2, placing methyl groups on lysine 27 of histone 3, typically tri-methylation (H3K27me3), to repress transcription (Czermin, Melfi et al., 2002, Müller, Hart et al., 2002). EZH2 is essential for embryonic development (Carroll,

Erhardt et al., 2001). In addition, EZH2 has frequent activating mutations in germinal centre and follicular DLBCL and is a promising therapeutic target (Kim & Roberts, 2016, Morin, Johnson et al., 2010). Surprisingly, while aberrant regulation of histone modifications has been implied in WM pathogenesis (Roccaro, Sacco et al., 2010), the role of EZH2 is yet to be investigated.

In this study, we sought to examine the role of BLIMP1 in WM, and its potential interplay with EZH2 in the disease. We demonstrate for the first time a role for BLIMP1 in regulating WM cell survival and in maintaining EZH2 protein levels. We identify a large overlap in transcriptional targets of the two factors but only a small degree of proximal binding of BLIMP1 with the H3K27me3 mark, implying that the factors repress transcription on an overlapping set of genes in parallel fashion. Finally, we reveal novel roles for BLIMP1 and EZH2 in evasion from natural-killer (NK) cell mediated cytotoxicity.

Results

BLIMP1 is important for cell survival in Waldenström's macroglobulinemia

As BLIMP1 is expressed in $CD19^{+}$ cells in a subset of WM patients (Roberts et al., 2013, Zhou et al., 2014), and given its roles in myeloma and DLBCL, we wanted to determine whether it plays a role in WM. Interestingly, in published transcriptome profiles from WM patients, the mRNA levels of *PRDM1*, the gene encoding BLIMP1, were elevated in WM cells from patients carrying the the $MYD88^{L265P}$ mutation (Hunter, Xu et al., 2016), which is associated with poorer prognosis in WM compared to $MYD88^{WT}$ (Treon, Cao et al., 2014). This suggests that BLIMP1 expression is induced downstream of $MYD88^{L265P}$. As BLIMP1 is known to be expressed in myeloma cell lines, we compared its expression in the myeloma cell line OPM-2 to that of the three WM cell lines RPCI-WM1 (RP), MWCL-1 (MW) and BCWM.1 (BC) by immunofluorescence staining (Fig 1A). All the cell lines expressed BLIMP1, with the RP cells showing relatively uniform expression levels in all cells. However, the MW and BC cells showed more heterogeneous protein levels, with 43% of MW and 18% of BC cells expressing BLIMP1 above background levels. The heterogeneity

of BLIMP1 expression in these cell lines does not rule out its importance, as the symptomatic antibody-secreting compartment is likely driven by BLIMP1. To examine the potential role of BLIMP1 in WM, we engineered the RP cell line with two distinct doxycycline (dox)-inducible artificial miRNAs targeting the *PRDM1* mRNA (*PmiR1 and PmiR2)* to knock-down (KD) BLIMP1 or a non-targeting control miRNA (*NTmiR*). The induction of *PmiR1* and *PmiR2* led to a 76% and 60% decrease in BLIMP1 protein respectively (Fig 1B). We also used *PmiR1* to engineer MW cells leading to a 60% reduction in BLIMP1 protein levels (Fig 1C).

BLIMP1 KD in WM cells led to decreased cell survival, with 62% and 71% live cells remaining in RP and MW cell cultures respectively 48h post dox addition, (Fig 1D) and only 3% viable cells remaining in RP cultures at five days after *PmiR1* induction. Despite an initial decrease in viability, by day 5, MW cells recovered their viability, likely due to cells without BLIMP1 KD overtaking the culture as a uniform knock-down in all the cells was not obtained. The proportion of apoptotic cells went up in RP cells by 2.64 and 2.25-fold upon *PmiR1* and *PmiR2* induction respectively, (Fig EV1A). While BLIMP1 KD led to a decrease in viability of MW cells as described above, the increase in apoptosis levels at 48 h did not reach statistical significance (Fig EV1B). The smaller effect of BLIMP1 KD in the MW cell line could be due to having a lower degree of KD in these cells, or because of the high proportion of cells lacking high levels of BLIMP1. Attempts at knocking down BLIMP1 in the BC cell line were inconclusive due to the lack of stable miR transduction and maintenance, presumably because of leakiness of miR expression from the inducible promoter.

We performed a genetic complementation test, where RP *PmiR1* cells were transduced with a lentivirus harbouring either *PmiR1*-resistant BLIMP1-EGFP encoding cDNA or EGFP (Lois, Hong et al., 2002) (Fig 1E). Crucially, this revealed that the decrease in cell viability could be rescued in cells transduced with miR-resistant BLIMP1 (81% viable cells, normalized to BLIMP1-transduced *NTmiR* RP cells) compared to the EGFP control (65% viable cells, normalized to BLIMP1-EGFP-transduced *NTmiR* cells) at 48h post BLIMP1-KD induction (Fig 1F). At five days post BLIMP1-KD induction 57% of the BLIMP1-transduced cells were viable compared to only 3% of the EGFP-transduced cells (Fig 1F). Additionally, 5 days

post KD, the miR resistant BLIMP1-transduced cells were still viable (23% resazurin reduction) compared to EGFP-transduced cells (6%) (Fig 1G). Together, these data show that BLIMP1 is a survival factor in WM cells, and that BLIMP1-mediated viability is likely due to the suppression of apoptosis. This is in line with previous findings of BLIMP1 suppressing apoptosis in myeloma through its interaction with Aiolos (Hung, Su et al., 2016).

BLIMP1 expression maintains EZH2 protein levels

The expression of BLIMP1 is induced by MYD88, among other factors. MYD88 is necessary for initiation of the antiviral germinal centre (GC) response (Hou, Saudan et al., 2011). The GC reaction is the mechanism by which B cells undergo somatic hypermutation and class switch recombination in order to increase their affinity to antigens (Basso & Dalla-Favera, 2015). Another essential factor in the GC reaction is the histone methyltransferase EZH2, which drives proliferation of GC B cells (Béguelin, Popovic et al., 2013). Furthermore, EZH2 is necessary for the early T-independent development of plasma cells in response to a viral antigen (Guo et al., 2018). As several lines of evidence from studies of mouse plasmablasts and PGCs show a functional overlap and perhaps a direct interaction between BLIMP1 and EZH2, we sought to investigate the potential interplay between the two factors in WM (Kurimoto et al., 2015, Magnúsdóttir et al., 2013, Minnich et al., 2016). Our first line of inquiry revealed a decrease in EZH2 expression upon BLIMP1 KD in RP cells (Fig 2A). Interestingly, this result was replicated in OPM-2 multiple myeloma cells harbouring *PmiR1* (Fig 2B). Simultaneous transduction of RP cells with the miR-resistant BLIMP1 construct as above (Fig 1E) restored EZH2 protein levels, confirming the specificity of the KD (Fig 2C, quantified in Fig EV2A). Furthermore, the signal intensities of BLIMP1 and EZH2 within approximately 2×10^4 individual nuclei were positively correlated in two separate experiments ($R^2 = 0.338$, $R^2 = 0.684$). These experiments for the first time, uncover a dependency of EZH2 on BLIMP1 expression.

We then sought to understand the mechanism by which BLIMP1 maintains EZH2 protein levels. To this end, we performed quantitative reverse transcription PCR (RT-qPCR) comparing *PmiR2* to *NTmiR* RP cells upon BLIMP1 KD induction. Consistent

with the loss of BLIMP1 protein, we saw a potential increase in steady state *PRDM1* levels due to the loss of BLIMP1 auto-repression (Martins & Calame, 2008) (Fig 2D). However, *EZH2* mRNA levels were not decreased in the RP cell line showing that the loss of EZH2 downstream of BLIMP1 KD is at the post-transcriptional level in this cell line (Fig 2D). The levels of *EZH2* mRNA were slightly decreased in OPM2 myeloma cells (Fig 2E). However, when we treated RP *PmiR1* cells with the proteasome inhibitor MG-132, the EZH2 protein levels were restored to the same levels as that of *NTmiR* cells also treated with proteasome inhibitor (Fig 2F,G). This reveals that the modulation of EZH2 levels by BLIMP1 occurs through the inhibition of proteasome mediated protein degradation.

As EZH2 is known as a key driver of cancer cell transformation (Béguelin et al., 2013, Kleer, Cao et al., 2003) and can play a role in preventing apoptosis (Wu, Zheng et al., 2009), we sought to determine if BLIMP1 mediated WM cell survival is dependent on EZH2. To test this, we genetically complemented the loss of BLIMP1 in the RP *PmiR1* cells by lentiviral transduction of an EZH2 expression construct (Fig 2H). However, the restoration of EZH2 levels did not confer an increase in viability to the BLIMP1 KD cells, with only 2% viable cells remaining 5 days post BLIMP1-KD induction (Fig 2I). Consistent with this, the EZH2-specific catalytic inhibitor tazemetostat did not affect RP cell viability even over a 96 h period (Fig EV2B), despite a dose dependent decrease in H3K27me3 levels (Fig EV2C). Thus, BLIMP1 maintains WM cell survival independently of EZH2.

BLIMP1 KD induces large transcriptional changes

In order to investigate the molecular mechanisms underpinning the above phenotypic observations, we examined the global gene expression changes induced by BLIMP1 KD. We performed transcriptome profiling of the RP *PmiR2* and *NTmiR* cell lines following 48 h of dox treatment. We profiled *PmiR2* rather than the *PmiR1* cells because the lower extent of cell death made them more suitable for RNAseq library construction. Using a q-value cutoff of 0.05, we identified 7814 differentially expressed genes between *PmiR2* and *NTmiR* (Fig 3A and EV Table 1).

As BLIMP1 is the key repressor of the B cell transcriptional program during plasma cell differentiation (Kallies, Hasbold et al., 2004, Minnich et al., 2016, Shaffer et al., 2002, Shapiro-Shelef et al., 2003), we asked whether this mechanism was perturbed in WM where the differentiation process is somewhat halted. Previously characterized B cell lineage targets of BLIMP1, including *CIITA* (Chen, Gilbert et al., 2007, Piskurich, Lin et al., 2000a), *PAX5* (Lin, Angelin-Duclos et al., 2002), *SPIB* and *BCL6* (Shaffer et al., 2002) showed significantly increased expression following BLIMP1 KD (Fig 3B), suggesting that they are repressed by BLIMP1 in WM cells. However, other BLIMP1 targets such as *MYC* (Lin, Wong et al., 1997) and *ID3* (Shaffer et al., 2002) were unaltered. On the other hand, the plasma cell transcription factor *IRF4*, which is important for cell survival in multiple myeloma (Shaffer, Emre et al., 2008), was previously shown to be activated downstream of BLIMP1 in plasma cells (Minnich et al., 2016). Curiously, here we observed it to be induced downstream of BLIMP1 repression and therefore repressed by BLIMP1. Interestingly, and highly relevant to WM pathogenesis and treatment, the BTK inhibitor, *IBTK* was induced upon BLIMP1 KD. The inhibition of BTK via Ibrutinib is now a common treatment modality in WM (Gertz, 2019). Taken together, BLIMP1 does appear to be repressing most but not all of its canonical B cell targets in RP cells. To examine the pro-apoptotic effect of BLIMP1 KD in the RP cell line, we looked at the expression profiles for key apoptosis genes. In line with the phenotype, we observed a large number of apoptosis genes with significantly increased expression following BLIMP1 KD. These included *MAP3K5* (*ASK1*), *XAF1*, *CASP4*, *CASP8*, *FAS*, *DFFA*, *JUN* and *BCL2L11* (*BIM*) amongst others (Fig 3C). Finally, we observed a significant de-repression of the *SMURF2* mRNA (EV3A). SMURF2 is an E3 ubiquitin ligase known to target EZH2 for proteasome-mediated degradation and could thus contribute to the decrease in EZH2 protein levels upon the loss of BLIMP1 (Yu, Chou et al., 2013). Taken together, BLIMP1 KD induces extensive gene expression changes in RP including the de-repression of B cell- and apoptosis-related genes, as well as *SMURF2*.

BLIMP1 and EZH2 transcriptionally regulate overlapping pathways

Because of the suggested BLIMP1-EZH2 regulatory relationship (Guo et al., 2018, Magnúsdóttir et al., 2013, Minnich et al., 2016), we wanted to determine to which

extent the transcriptional changes brought about by BLIMP1 are dependent on EZH2 catalytic activity. We treated RP cells with the EZH2 catalytic inhibitor, tazemetostat, or DMSO and performed genome wide expression profiling to uncover 450 differentially expressed genes (Fig 3D and EV Table 2). There was an overall smaller amplitude of change for individual genes compared to the changes induced by BLIMP1 KD (Fig EV2C). Nevertheless, there was a highly significant overlap between transcripts increased in *PmiR2* vs. *NTmiR* and in tazemetostat vs. DMSO treated cells (184 genes, p = 1.8e-37) (Fig 3E). Meanwhile, transcripts that showed decreased expression, i.e. genes activated by BLIMP1 or EZH2, overlapped to a much smaller extent, in line with the smaller number of transcripts decreasing in expression with tazemetostat treatment (Fig 3F). Tazemetostat treatment did not induce the same amplitude or extent of transcriptional changes of B cell genes as BLIMP1 KD did, although a number of genes were still significantly de-repressed, including *PIK3CD*, *CCR7* and *ID3* (Fig 3G). Furthermore, consistent with EZH2 inhibition not causing alterations in cell survival, fewer apoptosis genes were differentially expressed compared to the BLIMP1 KD, however a number of apoptosis genes were de-repressed, including *XAF1*, *CASP4*, *FAS* and *JUN* (Fig 3H).

To investigate the pathways jointly regulated by BLIMP1 and EZH2, we performed gene set enrichment analysis using the Hallmarks collection of gene sets (Liberzon, Birger et al., 2015, Subramanian, Tamayo et al., 2005). A number of gene sets were positively enriched with BLIMP1 KD, including interferon and TNFα responses, apoptosis and the inflammatory response (Fig EV3B). These gene sets are consistent with previous studies demonstrating BLIMP1-mediated repression of interferon responsive genes and apoptosis (Doody, Stephenson et al., 2007, Elias, Robertson et al., 2018a, Hung et al., 2016, Lin et al., 2007, Tooze et al., 2006). Additionally, the unfolded protein response and mTORC1 signalling gene sets were depleted upon BLIMP1 KD (Tellier et al., 2016). Transcriptional changes upon tazemetostat treatment were positively enriched for overlapping sets of genes with BLIMP1 KD, including interferon and TNFα responses (Fig EV3C). While far fewer gene sets were depleted in expression upon tazemetostat treatment, they all overlapped with that of the BLIMP1 KD depleted sets. This suggests that pathways involved in the immune response may be regulated in concert by BLIMP1 and EZH2.

Collectively, the transcriptomic analyses demonstrate a large overlap in targets of repression by BLIMP1 and EZH2, highlighting the interplay of the two factors.

BLIMP1 binds to a set of H3K27me3 marked genes at a distance from the mark

Given the large overlap in transcriptional targets and pathways identified above, and the previously published overlaps in genome wide binding of EZH2 and BLIMP1, we next sought to define their direct genomic targets. This should help distinguish gene expression changes resulting from BLIMP1's effect on EZH2 stability, or if BLIMP1 might recruit EZH2 to chromatin.

To this end we performed chromatin immunoprecipitation coupled to deep sequencing (ChIPseq) for H3K27me3, the histone modification catalysed by EZH2, and BLIMP1 in the RP cell line. We identified 14813 peaks for the H3K27me3 mark (EV Table 3), assigned to 4198 genes (EV Table 4), whereas 505 BLIMP1 peaks were identified (EV table 5), assigned to 841 genes (EV Table 6). The previously identified DNA binding motif for BLIMP1 (Kuo & Calame, 2004) was enriched by *de novo* motif analysis in the called BLIMP1 peaks, validating the quality of the experiment (Fig EV4A). Peaks were mapped relative to their assigned transcription start sites (TSS) for BLIMP1 (Fig EV4B) and H3K27me3 (Fig EV4C).

If BLIMP1 recruits EZH2 to chromatin in WM cells, as is suggested in mouse plasmablasts (Minnich et al., 2016), we hypothesised that a large proportion of BLIMP1 peaks would be located in close proximity to H3K27me3 marks. However, only 42 peaks from each factor were present at sites within 10 kb of each other, and this overlap was not statistically significant (Fig 4A). When we plotted signal for H3K27me3 at ± 3 kb flanking BLIMP1 peaks, only a small level of enrichment was observed (Fig 4B). However, when we assigned the peaks from the respective experiments to genes, a significant overlap of 261 genes emerged between BLIMP1 and H3K27me3 in RP cells (Fig 4C), including B-cell genes *PIK3CD* and *POU2F2 (OCT2)*, the STAT1 activator *RNF19B* (*NKLAM*) (Lawrence & Kornbluth, 2016), and the cell-growth inhibitor *NUB1* (Fig 4D).

To test whether these findings can be applied more generally than only to WM cells, we performed ChIPseq for BLIMP1 and H3K27me3 in the OPM-2 (EV Tables 7-10) and NCI-H929 (EV Tables 11-14) myeloma cell lines as well as ChIPseq for EZH2 in NCI-H929 cells (EV Tables 15-16) to reveal the direct binding sites for EZH2, rather than just the polycomb mark. As before, the BLIMP1 consensus binding motif was identified within the called peaks by *de novo* motif analysis (Fig EV4D). When we mapped the peaks relative to their TSS for BLIMP1 (Fig EV4E), H3K27me3 (Fig EV4F) and EZH2 (Fig EV4G), we observed a strong enrichment of signal over TSSs. Interestingly, both the multiple myeloma cell lines displayed a much stronger enrichment of H3K27me3 over TSSs than the RP WM cell line, indicating that H3K27me3 is more often present at distal sites in the RP cell line. There was a strong enrichment for BLIMP1 binding in the OPM-2 and NCI-H929 cell lines over sites bound by BLIMP1 in the RP cell line (Fig EV4H), showing that BLIMP1 binds to mostly the same sites in WM and multiple myeloma. Contrastingly, we observed less enrichment of the H3K27me3 mark in the OPM-2 and NCI-H929 cell lines over sites marked by H3K27me3 in the RP cell line (Fig EV4I). This corresponds to the different enrichments of H3K27me3 over TSSs in th RP cells compared to the myeloma cell lines, suggesting that H3K27me3 has a different distribution in WM compared to myeloma. Interestingly, *SMURF2* was one of the genes bearing both BLIMP1 peaks and the H3K27me3 mark in the RP cell line (Fig EV4J). As with the RP cells, we rarely observed peaks within a 10kb distance of one another when comparing BLIMP1 and H3K27me3 (Fig EV4K) or BLIMP1 and EZH2 (Fig EV4L) in the OPM-2 and NCI-H929 cell lines. When we plotted the distribution of the H3K27me3 mark and EZH2 over BLIMP1 peaks in NCI-H929 cells there was a small level of enrichment of the H3K27me3 mark flanking the BLIMP1 peaks, which is more likely to reflect general histone distribution than a specific enrichment of the H3K27me3 mark, given the paucity of called H3K27me3 peaks in the proximity of BLIMP1 binding (Fig 4E). Again, we observed a higher degree of overlap between genes assigned to peaks for the respective factors, with a statistically significant overlap between genes bound by BLIMP1 and H3K27me3 in NCI-H929 cells, but not OPM-2 cells (Fig EV4M). Genes bound both by BLIMP1 and EZH2 were not statistically over-represented (Fig EV4N). The above analyses reveal that the majority of BLIMP1 and EZH2 binding to chromatin occur at

relatively distal sites between the two factors and their direct regulation on chromatin is therefore unlikely to be due to a direct physical interaction.

In order to determine the direct transcriptional targets of BLIMP1 and EZH2, we compared our ChIPseq and transcription profiling data from the RP cell line. There were 231 and 120 genes associated with BLIMP1 binding that were either induced or repressed upon BLIMP1 KD respectively (Fig 4F-G), in line with previous observations showing that BLIMP1 has a stronger effect in gene repression than activation (Magnúsdóttir et al., 2013, Magnúsdóttir et al., 2007, Minnich et al., 2016, Shaffer et al., 2002). Conversely there were 118 genes associated with the H3K27me3 mark that were induced upon tazemetostat treatment (Fig 4H), but only 7 genes with decreased expression overlapped (Fig 4I). Overall, only approximately 3% of genes marked by H3K27me3 were de-repressed following tazemetostat treatment in these experiments. This indicates that inhibition of EZH2's catalytic activity alone is insufficient to activate most H3K27me3 targets. Meanwhile, approximately one third of BLIMP1-bound genes were direct targets of transcriptional repression, indicating that BLIMP1 binding actively maintains gene repression. Taken together, as BLIMP1 and H3K27me3 are largely present at distinct sites from one another, a great extent of their co-operation is likely through their binding to different sites on the same genes, as well as through BLIMP1 maintenance of EZH2 protein levels.

BLIMP1 represses transcription of immune surveillance and signalling molecules in concert with EZH2

As gene sets in immune signalling pathways were the most highly enriched upon BLIMP1 KD and EZH2 inhibition, we looked further into the biological significance of these insights. Indeed, immune signalling genes differentially expressed upon BLIMP1 KD can be divided into three mechanistic categories. First, BLIMP1 represses the expression of genes encoding surface ligands that activate T and NK cells, including *ICOSLG*, *TNFSF9*, *CD48*, *MICA*, *CLEC2B*, *ICAM1* and *ITGAM* (Pardoll, 2012, Vivier, Tomasello et al., 2008), MHC class II molecules including *HLA-DMA*, *HLA-DMB* and *CD1D*, along with Class II transactivator (*CIITA)*, and the immune synapse molecule *CAV1* (Fig 5A). Furthermore, MHC class I pathway members, *HLA-A* and *HLA-B* are decreased with BLIMP1 KD, in contrast to previous

studies (Doody et al., 2007, Mould, Morgan et al., 2015). Second, BLIMP1 represses both immune-checkpoint inhibitory ligands and their receptors, which are de-repressed in the cells with BLIMP1 KD. These include *TNFRSF14* and *BTLA*, *HAVCR2* and *LGALS9* (Pardoll, 2012, Vivier et al., 2008). Additionally, inhibitory ligands whose receptors are not differentially expressed are also repressed by BLIMP1, including PD-L2, with BLIMP1 binding just downstream of the *PDCDLG2* gene (Fig EV5A). Of note, the PD-1 receptor encoded by *PDCD1* can also have an inhibitory effect on B cell activation (Thibult, Mamessier et al., 2013), and is expressed at a comparable level to its ligand in the RP cell line. The third mechanistic category repressed by BLIMP1 includes genes involved in the repression of downstream signalling from cytokines such as interferons and TNFα. The receptor-encoding genes *IFNGR1*, *IFNAR1*, *IFNLR1*, *TNFRSF1A* and *TNFRSF1B* are all de-repressed upon BLIMP1 KD. So too are downstream players in interferon signalling, *JAK1*, *STAT1*, *STAT2*, *IRF9* and *IFIT1*-3 and *OAS1-3*, as well as TNF pathway members *MAP3K5*, *CASP8* and *CASP9*, which are also apoptosis mediators (Fig 3C).

Around half of the genes discussed above were also significantly changed with tazemetostat treatment (Fig EV5B), including *NCR3LG1*, *CD48*, *LILRB1*, *PDCD1LG2*, *LGALS3* and *STAT1*. Interestingly, while none of the surface molecule genes except for *PDCDLG2* were bound by BLIMP1, some were enriched for H3K27me3 (Fig 5B). Whereas the downstream signalling effectors, *IFIT2* and *STAT1*, were bound by BLIMP1 (Fig 5C), consistent with previous findings in mammary epithelial cells (Elias, Robertson et al., 2018b). In addition, a number of these differentially expressed genes did not bear either H3K27me3 or BLIMP1, and so are likely regulated by secondary effectors or through distal enhancers.

Next, we sought to determine if the genes bearing H3K27me3 marks but not bound by BLIMP1 are repressed by BLIMP1 via the maintenance of EZH2. Using EZH2 overexpression in RP cells with BLIMP1 KD, we performed qPCR and observed that repression of the B cell genes *RCAN3, ZFP36L1* and *CIITA* was restored (Fig EV5C). Furthermore, the repression of the immune inhibitory checkpoint ligand *TNFRSF14* and the inhibitory receptor *HAVCR2* was restored upon restoration of EZH2 levels. By comparison, BLIMP1 targets not bearing the H3K27me3 mark such as *STAT1* and *TFEC* were not altered upon EZH2 restoration.

Taken together, BLIMP1 and EZH2 repress the transcription of genes that mediate killing by NK or T cells, inhibitory receptors and their ligands, as well as cytokine receptors and downstream responders. A subset of these targets are regulated by BLIMP1 through EZH2 maintenance, whereas others are regulated independently of EZH2.

BLIMP1 confers evasion from NK cell-mediated cytotoxicity

The transcriptional changes above suggested that BLIMP1 and EZH2 were repressing cytotoxic synapse molecules and receptors, which may lead to escape from immune surveillance. We hypothesised that the KD of BLIMP1 or inhibition of EZH2 could lead to differential activation of NK cell-mediated cytotoxicity. Towards this, we isolated NK cells from human blood and co-cultured them with RP cells treated to induce BLIMP1 KD or with tazemetostat. We assessed NK cell degranulation by staining the NK cells for the expression of CD107a (also called LAMP-1), which appears on the cell surface upon degranulation. Negative and positive controls are shown in Fig EV5D. The NK cells co-cultured with *PmiR1* RP cells showed a significant increase in the frequency of $CD107a^{+}$ cells compared to that when co-cultured with *NTmiR* cells, revealing the sensitisation of NK-cells to WM cells upon BLIMP1 KD (Fig 5D-E). Tazemetostat treatment failed to induce changes in NK-cell degranulation, perhaps reflecting its relatively smaller effect on gene expression compared to that of BLIMP1 KD. However, when we measured the effect of BLIMP1 KD or EZH2 inhibition on NK cell-mediated cytotoxicity of RP cells by the level of cytolysis, both BLIMP1 KD and tazemetostat treatment induced statistically significant increases in NK cell-mediated cytotoxicity (Fig 5F). As such, EZH2 inhibition does not appear to affect NK cell activation, with no change in the degranulation of NK cells cultured with DMSO- or tazemetostat-treated RP cells. However, it may sensitise WM cells to cell-mediated cytotoxicity. Collectively, these data indicate that BLIMP1 and EZH2 mediated transcriptional repression drives escape from immune surveillance in WM.

Discussion

BLIMP1, a key driver of plasma cell terminal differentiation has as of yet not been extensively studied studied in WM, despite it's crucial role for antibody secretion (Minnich et al., 2016, Shapiro-Shelef et al., 2003). Antibody secretion is a critical aspect of WM pathology, since a large proportion of WM symptoms are caused by high IgM serum levels (Treon, 2009). In this study we show for the first time direct evidence for the importance of BLIMP1's role in WM cell survival. We further show that BLIMP1 maintains the protein levels of the histone methyltransferase EZH2, demonstrating that the functional interaction between BLIMP1 and EZH2 is more complex than previously thought (Guo et al., 2018, Kurimoto et al., 2015, Magnúsdóttir et al., 2013, Minnich et al., 2016). Furthermore, our scrutiny of the genes regulated by BLIMP1 and EZH2 revealed that the factors collaborate in the evasion of immune surveillance mechanisms. This was evidenced by enhanced degranulation of NK cells co-cultured with BLIMP-1 KD WM cells, as well as enhanced NK cell-mediated WM cellular cytotoxicity upon either BLIMP KD or EZH2 inhibition.

Our finding that BLIMP1 promotes survival in WM cells provides new insight into WM pathology and potentially its aetiology. BLIMP1 is activated downstream of MYD88 signalling in B cells (Pasare & Medzhitov, 2005), and BLIMP1 expression is increased in tumours harbouring the $MYD88^{L265P}$ activating mutation in WM (Hunter et al., 2016). However, $MYD88^{L265P}$ tumours have an increased frequency of heterozygous deletions in the 6q locus containing *PRDM1* (Schop et al., 2002). This is particularly interesting in light of findings showing that high levels of BLIMP1 tend to inhibit proliferation, whereas intermediate levels promote survival and immunoglobulin (Ig) secretion (Kallies et al., 2004, Nutt, Fairfax et al., 2007). Placed in the context of our findings, we can speculate that perhaps the loss of one copy of the *PRDM1* gene upon MYD88 constitutive activation dampens the anti-proliferative effect of BLIMP1 while still maintaining its positive effect on survival and Ig secretion. Indeed, our results demonstrate decreased cell viability with BLIMP1 KD even for the MW cell line that expresses low BLIMP1 levels. It is also interesting to speculate that a complete loss of BLIMP1 during tumorigenesis would more likely

490 result in B cell lymphoma (Pasqualucci et al., 2006), but the loss of Ig secretion
491 ability and plasma cell differentiation would preclude WM tumour formation.
492
493 A first line of treatment in WM is rituximab therapy, targeting the B cell
494 specific surface molecule CD20. However, the cells remaining after this treatment
495 present one of the biggest challenges in WM therapy, and rituximab is not
496 recommended for patients exhibiting high serum IgM levels (Gavriatopoulou, Musto
497 et al., 2018). This highlights the importance of the plasma cell compartment in WM,
498 which is likely maintained by BLIMP1. Furthermore, our results demonstrate
499 repression of *IBTK*, an inhibitor of BTK signaling, by BLIMP1, providing a
500 mechanism by which BLIMP1 may potentiate BTK signaling downstream of MYD88
501 activation. The inhibition of BTK by Ibrutinib is another WM therapy that results in a
502 dramatic reduction in WM symptoms (Treon, Tripsas et al., 2015).
503
504 A key question addressed in this study was in elucidating the interplay of
505 BLIMP1 and EZH2 in WM. BLIMP1 shows an overlapping binding pattern with
506 EZH2 in mouse PGCs implicating an interaction between these factors in epigenetic
507 reprogramming during differentiation (Kurimoto et al., 2015, Magnúsdóttir et al.,
508 2013). This implication was expanded in mouse plasmablasts with the discovery that
509 BLIMP1 physically interacts with EZH2, directing the placement of H3K27me3 to
510 repress B cell genes during the transition to plasma cells (Minnich et al., 2016). In
511 addition, EZH2 aids in the generation of antibody-secreting plasma cells in the mouse
512 and represses BLIMP1 target genes (Guo et al., 2018). Here, we demonstrate that
513 BLIMP1 maintains EZH2 protein levels which could at least in part explain the
514 overlap in transcriptional targets seen by Guo et al. (Guo et al., 2018) in mouse
515 plasmablasts, beyond the mechanism of BLIMP1 potentially recruiting EZH2 to
516 chromatin. However, it is interesting to speculate that the BLIMP1-EZH2 interaction
517 is necessary for normal epigenetic reprogramming during the B cell to plasma cell
518 transition, and the perturbation of this interaction may contribute to the aetiology of B
519 cell malignancies. Interestingly, the restoration of EZH2 levels did not improve cell
520 survival following BLIMP1 KD, indicating that the requirement for BLIMP1 in
521 mediating WM cell survival is through other mechanisms rather than its effect on
522 EZH2.
523

While both multiple myeloma and normal plasma cells rely on BLIMP1 for their survival (Lin et al., 2007, Shapiro-Shelef et al., 2003, Shapiro-Shelef, Lin et al., 2005) , EZH2 expression is decreased as post-germinal centre B cells transition to plasma cells (Croonquist & Van Ness, 2005, Zhan, Tian et al., 2003), whereas many multiple myeloma cell lines are reliant on EZH2 for cytokine independent growth and thus their more aggressive plasma cell leukemia phenotype (Croonquist & Van Ness, 2005, Hernando, Gelato et al., 2016). Our results indicate that the effects of BLIMP1 on EZH2 levels might extend to myeloma, and perhaps other tumours where the two factors are co-expressed, and warrants further study.

Immune evasion is most extensively studied in relation to solid tumours, but in cancers of immune system cells, the paradigm is somewhat different. Lymphocytes interact with other cells of the immune system not only when they are abnormal, such as in cancer, but also to receive stimulatory and inhibitory signals, regulating their own immune response (de Charette & Houot, 2018). In WM, PD-1 signaling from secreted ligands inhibits T cell responses (Jalali, Price-Troska et al., 2018), but other mechanisms of immune evasion have not been investigated. Our results demonstrate for the first time that BLIMP1 and EZH2 mediate evasion from NK cell surveillance. This occurs both in terms of NK cell activation and cytotoxicity against WM cells downstream of BLIMP1. Meanwhile, the effect of EZH2 inhibition is restricted to NK-cell mediated cytotoxicity without activation of the NK cells themselves. Based on our transcriptomic profiling, the main mechanism by which BLIMP1 promotes immune evasion in WM is likely to be “hiding” from cytotoxic lymphocytes by transcriptional repression of activating ligands. Whereas, EZH2 is more likely to be de-sensitising WM cells to external cytotoxicity-inducing signals. Interestingly, in melanoma EZH2 promotes evasion from IFNγ-producing cytotoxic T cells (Zingg, Arenas-Ramirez et al., 2017). Investigation into the use of EZH2 inhibition for sensitising WM and other cancer cells to immune-mediated killing should be considered for prospective therapies.

In conclusion, we provide key evidence for a crucial role of BLIMP1 in promoting WM cell survival. In the WM cell context, we discover that BLIMP1 maintains EZH2 protein levels. We show cooperation between BLIMP1 and EZH2 in the repression of immune surveillance genes, among others. Finally, we find that

BLIMP1 confers evasion from NK-cell mediated cytotoxicity. In future studies it would be important to investigate the intricate interplay between BLIMP1 and EZH2 in cancers to expand their therapeutic potential.

Materials and Methods

Suspension cell lines

RPCI-WM1 (a gift from Prof. Asher A. Chanan-Khan), BCWM.1 (a gift from Prof. Steven P. Treon) and OPM-2 (#ACC50, Leibniz Institute DSMZ) cell lines were maintained in RPMI media (#SH30255.FS, Hyclone, GE Healthcare Biosciences) supplemented with 10% foetal bovine serum (FBS) (#SV30160.03, Hyclone, GE Healthcare Biosciences, Denmark). The MWCL-1 (a gift from Stephen M. Ansell) and NCI-H929 (#ACC163, Leibniz Institute DSMZ) cell lines were maintained in RPMI media supplemented with 10% FBS 1mM sodium pyruvate (#SH30239.01, Hyclone GE Healthcare Biosciences) and 50µM beta-mercaptoethanol (#0482, VWR).

Cloning

For knock-down of BLIMP1, artificial miRNA sequences were designed to target the *PRDM1* transcript using the RNAiDesigner tool (Thermo Fisher). These were named *PmiR1* and *PmiR2*. A non-targeting control miRNA (*NTmiR*) was also used as previously described (Hackett, Sengupta et al., 2013). The miRNA sequences were cloned into the tetracycline-inducible pPB-hCMV*1-miR plasmid (Hackett et al., 2013, Murakami, Günesdogan et al., 2016). See Appendix Table 1 for miRNA sequences.

Site directed mutagenesis was used to introduce mutations in coding sequence of the FUW-PRD1-BF1 lentiviral expression construct (Magnúsdóttir et al., 2007) to render it resistant to the targeting miRNAs. The plasmid was amplified using primers listed in Appendix Table 2. FUW-EZH2 was derived first by PCR amplification from the pCMVHA-hEZH2 plasmid (Bracken, Pasini et al., 2003), then incorporated via Gibson assembly (New England Biolabs) into the FUGW backbone (Lois et al.,

590 2002). The pCMVHA hEZH2 plasmid was a gift from Kristian Helin (Addgene
591 plasmid # 24230 ; http://n2t.net/addgene:24230 ; RRID:Addgene_24230).
592
593 **Construction of knock-down cell lines**
594
595 Knock-down cell lines were constructed via electroporation 220V, 350µF using Gene
596 Pulser XCell (Bio-Rad) with plasmids containing our miRNA as described above,
597 using the piggyBac transposon system with the piggyBac transposase, the reverse-
598 tetracycline transactivator and a tetracycline-inducible EGFP. Stable cell lines were
599 selected for with 0.5 mg/mL or 1 mg/mL G418 disulfate solution (#A6798,
600 Applichem) for either the RP and MW, or OPM-2 cells respectively for nine days.
601 The RP cells were seeded at a density of 0.5 cells per well in a 96-well plate and
602 clones with the highest KD were used for further analyses. MW and OPM-2 cells
603 were used as a pool of cells directly after antibiotic selection. miRNA expression was
604 induced with 0.2 or 0.5 µg/mL Doxycyline Hyclate (#sc-211380, Santa Cruz
605 Biotechnology) for either the RP and OPM-2, or MW cells respectively.
606
607 **Lentiviral transduction**
608
609 Lentivirus was produced by transient transfection of HEK293T cells with the
610 envelope vesicular stomatitis virus G protein (VSVG)-encoding pMD2.G plasmid, the
611 packaging plasmid psPAX2, and either the FUW-PRDI-BF1, FUW-EZH2 or FUGW
612 transfer plasmid. psPAX2 was a gift from Didier Trono (Addgene plasmid #12260;
613 http://n2t.net/addgene:12260; RRID:Addgene_12260). pMD2.G was a gift from
614 Didier Trono (Addgene plasmid #12259; http://n2t.net/addgene:12259;
615 RRID:Addgene_12259).
616 Viral supernatant was concentrated by ultracentrifugation using 100kDa Amicon
617 centrifugal filters (#UFC910008, Sigma-Aldrich). Suspension cell lines were
618 transduced by spinfection, 800 xg for 30 min with 8 µg/mL polybrene.
619
620 **Immunofluorescence staining**
621
622 Cells were cytospun onto glass slides for 3 min at 800 rpm. Samples were fixed and
623 permeabilised 10 min in 4% formaldehyde (#28906, Thermo Fisher Scientific), 0.1%

624 triton-X-100 (#T-9284, Sigma-Aldrich), then blocked for 1 h at room temperature
625 with 0.1% triton-X-100, 1% bovine serum albumin (#A1391, Applichem), and 10%
626 goat serum (#16210064, Gibco). Slides were incubated overnight at 4˚C with primary
627 antibody, anti-BLIMP1 (#9115, Cell Signaling Technologies) at a 1:100 dilution.
628 Nuclei were counterstained with 1µg/mL DAPI (#sc-3598, Santa Cruz
629 Biotechnology). The secondary antibody used was goat anti-rabbit Alexa Fluor 647
630 (#A21244, Thermo Fisher Scientific) at a 1:1000 dilution. The signal intensity within
631 nuclei was quantified using CellProfiler, with background signal subtracted
632 (Carpenter, Jones et al., 2006).
633
634 **Protein extraction, SDS-PAGE, and Western Blot**
635
636 Cells were lysed in protein sample buffer (60mM Tris pH 6.8, 2% SDS, 10%
637 glycerol, 0.01% bromophenol blue, 1.25% β-mercaptoethanol), at 95˚C for 5 min.
638 Benzonase nuclease (#sc-202391, Santa Cruz Biotechnology) was used to digest
639 chromatin before loading on SDS-PAGE gel. Western blotting was performed as
640 previously described (Burnette, 1981).
641
642 **RNA Isolation, cDNA synthesis and RT-qPCR**
643
644 Cells were lysed in TRIsure reagent (#BIO-38032, Bioline), and RNA was extracted
645 according to the manufacturer's instructions. cDNA was synthesised using the
646 GoScript Reverse Transcriptase system (#A5001, Promega), in combination with
647 dNTP mix (#R0191, Thermo Fisher Scientific), random primer 6 (#S1230S, New
648 England Biolabs), murine RNase inhibitor (#M0314S, New England Biolabs) and
649 1.25mM $MgCl_2$. RT-qPCR was performed using the SensiFAST SYBR Lo-Rox Kit
650 (#BIO-94020, Bioline) on the 7500 Real-Time PCR system (Applied Biosystems).
651 Relative quantitation was calculated according to the Pfaffl method (Pfaffl, 2001),
652 with *ACTB* and *PPIA* used as reference genes. Primer sequences are listed in
653 Appendix Table 3.
654
655 **Viability, reduction and apoptosis assays**
656

657 The percentage of live cells was determined by trypan blue exclusion assay (Gibco).
658 The per cent reduction was determined by resazurin assay, with resazurin sodium salt
659 (Santa Cruz Biotechnology) added 5h before the assay end-point, and absorbance
660 measured at 595 and 570nm. Per cent reduction was calculated relative to the fully
661 reduced form of resazurin, resorufin. See Appendix Methods for more details.
662 Apoptosis was assessed using APC-Annexin V (#550474, BD Biosciences) together
663 with Annexin V binding buffer (#556454, BD Biosciences). Staining was carried out
664 according to the manufacturer's instructions and assessed using the MACSQuant
665 analyser (Miltenyi Biotec).
666
667 **Proteasomal inhibition**
668
669 To test inhibition of the proteasome, RP *NTmiR* or *PmiR1* cells were treated with
670 5µM MG-132 (#sc-201270, Santa Cruz Biotechnology) for 4 h, 20 h post dox
671 addition.
672
673 **RNAseq**
674
675 The *PmiR2* and *NTmiR* RP cells were treated with 0.2µg/mL dox for 48h. RP cells
676 were treated with 300nM tazemetostat (EPZ-6438, #S7128, Selleckchem) or DMSO
677 for 48h. Total RNA was isolated using TRI-reagent (#AM9738, Thermo Fisher
678 Scientific) according to the manufacturer's instructions, then treated with HL-
679 dsDNase (#70800-201, ArcticZymes), and purified using the RNeasy MinElute
680 Cleanup Kit (#74204, Qiagen). RNAseq libraries were constructed using the NEB
681 NEBNext® Ultra™ Directional RNA Library Prep Kit for Illumina® (#E7420S, New
682 England Biolabs) in combination with the NEBNext® Poly(A) mRNA Magnetic
683 Isolation Module (#E7490S, New England Biolabs). Pooled samples were clustered
684 on paired-end (PE) flowcells using a cBot instrument (Illumina). Sequencing was
685 performed on Illumina HiSeq 2500 using the v4 SBS sequencing kits with a
686 readlength of 2x125 cycles plus a 6 base index read. Primary processing and base
687 calling was done using HCS and RTA. Demultiplexing and generation of FASTQ
688 files was performed using scripts from Illumina (bcl2fastq v.1.8).
689 RNAseq raw reads were trimmed using Trim Galore
690 (https://www.bioinformatics.babraham.ac.uk/projects/trim_galore/), and

691 pseudoaligned to the hg38 transcriptome and quantified using Kallisto (Bray,
692 Pimentel et al., 2016). Differential expression analysis was performed using the
693 likelihood ratio test in Sleuth (Pimentel, Bray et al., 2017), on a gene level, with a q-
694 value of 0.05, and a $\log_2$ fold-change of ±0.3 as a significance cutoff. Gene set
695 enrichment analysis using the Hallmarks collection of gene sets was run in pre-ranked
696 mode using a list of all detected genes (Liberzon et al., 2015, Subramanian et al.,
697 2005). The rank value was calculated as $-\log_{10}$(q-value) × (sign of fold change).
698
699 **ChIPseq**
700
701 Transcription factor ChIP for BLIMP1 and EZH2 was performed as previously
702 described (Boyer, Lee et al., 2005, Magnúsdóttir et al., 2013, Magnúsdóttir et al.,
703 2007). ChIP was carried out for BLIMP1, using 60µL rabbit polyclonal antibody
704 recognising the C-terminal region of BLIMP1 (Kuo & Calame, 2004) with 3×10^7
705 nuclei, crosslinked with 0.4% formaldehyde. For EZH2, ChIP was performed using
706 40µL anti-EZH2 (D2C9, #5246, Cell Signaling Technology) with 2×10^7 nuclei,
707 crosslinked with 1% formaldehyde.
708 Histone ChIP for pan-H3 and the H3K27me3 mark was performed as previously
709 described (Shaffer et al., 2008). ChIP was performed for pan-H3 using 3µL anti-
710 histone H3 (D2B12, #4620S, Cell Signaling Technology). For H3K27me3, ChIP was
711 performed using 5µg anti-H3K27me3 (#ab6002, Abcam). All histone ChIP
712 experiments were performed with 1×10^7 cells per ChIP, crosslinked with 0.4%
713 formaldehyde.
714
715 Sequencing was performed as described above. Raw ChIPseq reads were trimmed as
716 above and aligned to the hg38 genome using Bowtie2 (Langmead & Salzberg, 2012).
717 Peaks were called using MACS2 (Zhang, Liu et al., 2008), and tracks were visualised
718 using the UCSC genome browser (Kent, Sugnet et al., 2002). Enrichment over
719 BLIMP1 peaks, H3K27me3 peaks and TSSs was calculated and mapped using
720 Deeptools (Ramírez, Ryan et al., 2016). Overlapping regions were tested for
721 significance using the hypergeometric test in the ChIPPeakAnno package in R (Zhu,
722 Gazin et al., 2010). Overlapping genes were tested for significance using Fisher's
723 exact test in the GeneOverlap package in R (http://shenlab-sinai.github.io/shenlab-
724 sinai/).

725

726 **NK cell isolation**

727

728 NK cells were isolated from heparinised buffy coats obtained from healthy human
729 donors, who all provided informed consent, provided by the Icelandic Blood Bank
730 (ethical approval #06-068). PBMCs were first isolated by density gradient
731 centrifugation with Histopaque-1077 (#10771, Sigma-Aldrich), then NK cells were
732 purified by negative enrichment using the NK cell isolation kit (#130-092-657,
733 Miltenyi Biotech) according to the manufacturer's instructions. NK cells were
734 cultured overnight in RPMI media supplemented with 10% FBS and 10ng/mL IL-2
735 (R&D Systems).

736

737 **Degranulation Assay**

738

739 NK cells were co-cultured with pre-treated RP cells at a 10:1 ratio. Anti-CD107a-PE
740 (clone H4A3, BioLegend) was added to the co-culture media. For the positive control,
741 NK cells in co-culture with RP cells were treated with 2.5µg/mL phorbol 12-myristate
742 13-acetate and 0.5µg/mL ionomycin. After 1h of co-culture, 2µM monensin was
743 added to every sample and incubated for an additional 4h. Cells were stained with
744 anti-CD56-APC (clone CMSSB, EBioscience), fixed with 1% PFA and analysed on
745 the Sony SH800S flow cytometer. Data were analysed using FlowJo v10.

746

747 **Cytotoxicity Assay**

748

749 NK cells were co-cultured with pre-treated RP cells at a 20:1 ratio for 4h.
750 Cytotoxicity was assessed by measurement of the adenylate kinase activity in the
751 culture medium using the ToxiLight assay (#LT07-217, Lonza). Luminescence was
752 measured using a Modulus microplate reader (Promega). Values were normalised to
753 wells containing pre-treated RP cells without NK cells, and are presented as relative
754 luminescence units (RLU).

755

756 **Data availability**

757 RNAseq and ChIPseq data are available at
758 http://www.ebi.ac.uk/arrayexpress/experiments/E-MTAB-7739 under the accession
759 code: E-MTAB-7739.
760

761 ## Author contributions

762 EM conceived, designed and supervised the work. KJA, ABO, BA, GAT and AEL
763 performed and designed the experimental work. KNJ performed flow cytometric
764 analyses and contributed to experimental design. KJA performed the bioinformatics
765 analyses. JTB and IH contributed to critical methodologies. KA and EM wrote the
766 paper.
767

768 ## Conflict of interest

769 The authors declare that they have no conflicts of interest.
770

771 ## Acknowledgements

772 We thank Arnar Palsson and Dagny A. Runarsdottir for their advice on RNAseq data
773 analysis. We thank Jona Freysdottir and Sunnefa Yeatman Omarsdottir for their
774 advice on the isolation of NK cells. We also thank the group of Eirikur Steingrimsson
775 for many good discussions and advice on the project. We thank Dr. Roopsha
776 Sengupta for providing critical inputs and proof-reading the manuscript.
777
778

779 ## Funding

780 This work was supported by project grants from the Icelandic Centre for Research
781 (RANNIS) (grant no. 140950-051) and the Icelandic Cancer Society, a doctoral
782 fellowship from the University of Iceland, and grant from the University of Iceland
783 Eggertssjodur and funds from the COST Project EpiChemBio.
784

785 ## Figure Legends

786

787 **Figure 1:** BLIMP1 promotes survival of WM cells
788 **(A)** BLIMP1 expression in myeloma cell line OPM-2 and in WM cell lines RP, MW
789 and BC as detected by immunofluorescence staining, with bar graph representing

790 percentage of BLIMP1^{bright} cells. Scale bars represent 20µm. **(B)** Immunoblot of
791 BLIMP1 expression following 48h dox induction of RP cells expressing *NTmiR*,
792 *PmiR1* or *PmiR2*, with bar graph representing the quantity of BLIMP1 relative to
793 actin; ****p < 0.0001. **(C)** Immunofluorescence staining of BLIMP1 following 48h
794 dox induction in MW cells expressing *NTmiR*, *PmiR1* or *PmiR2*, with CellProfiler
795 quantification; p = 0.0228. **(D)** Percentage of live cells as determined by Trypan blue
796 exclusion assay in the RP and MW cell lines. RP, p = 0.0019; MW, p = 0.0162. **(E)**
797 Immunoblot depicting lentiviral ectopic expression of EGFP or BLIMP1-EGFP in the
798 RP *PmiR1* cells, next to the RP *NTmiR* cells. **(F)** The percentage of live RP *PmiR1*
799 cells with ectopic EGFP or BLIMP1-EGFP expression determined by the Trypan blue
800 exclusion assay normalised to the percentage of live cells following transduction of
801 RP *NTmiR* cells with EGFP or BLIMP1-EGFP. Day 2, *p = 0.0165; Day 5, ***p =
802 0.0003. **(G)** Per cent reduction as measured by resazurin assay for RP *PmiR1* cells
803 with EGFP or BLIMP1-EGFP, five days after dox induction. *p = 0.0208. All p-
804 values as determined by student's two-tailed t-test. All graphs plotted as mean of
805 three independent experiments, with error bars representing standard deviation.
806
807 **Figure 2:** BLIMP1 maintains EZH2 protein levels
808 **(A)** Immunoblot of BLIMP1 and EZH2 expression following 48h dox-induction of
809 RP cells expressing *NTmiR*, *PmiR1* or *PmiR2*, with quantification of signal relative to
810 actin in bar plot; ***p = 0.0002; ***p = 0.001; **p = 0.0027. **(B)** Immunoblot of
811 BLIMP1 and EZH2 expression following 48h dox-induction of OPM-2 cells
812 expressing *NTmiR* or *PmiR1*, with quantification of signal relative to actin in bar plot;
813 ****p < 0.0001; *p = 0.016. **(C)** Immunofluorescence staining of BLIMP1 and EZH2
814 expression following 48 h dox-induction of RP cells expressing *NTmiR* or *PmiR1*,
815 transduced with EGFP or BLIMP1-EGFP. Scale bars represent 20 µm. **(D)** RT-qPCR
816 results depicting relative mRNA expression of *PRDM1* and *EZH2* normalised to *PPIA*
817 and *ACTB* in the RP cell line and **(E)** in the OPM-2 cell line. **(F)** Immunoblot of
818 BLIMP1 and EZH2 expression following 24h dox-induction of RP cells expressing
819 *NTmiR* or *PmiR1* treated with DMSO or 5µM MG-132 for 4h. **(G)** The ratio of EZH2
820 expression relative to actin for RP *PmiR1* cells divided by RP *NTmiR* cells treated
821 with DMSO or MG132 as in Fig. 2F; p = 0.0134. **(H)** Immunoblot of BLIMP1 and
822 EZH2 expression following 48h dox-induction of RP *NTmiR* cells or *PmiR1* cells
823 transduced with EGFP or EZH2-EGFP. **(I)** Percentage of live cells as determined by

824 Trypan blue exclusion assay in the RP *PmiR1* cells transduced with EGFP or EZH2-
825 EGFP. All p-values as determined by student's two-tailed t-test. All graphs plotted as
826 mean of three independent experiments with error bars representing standard
827 deviation.
828
829 **Figure 3:** BLIMP1 KD induces large transcriptional changes
830 RNAseq results for **(A)** 48h dox-induced RP cells comparing *PmiR1* to *NTmiR*.
831 Values are plotted as $\log_2$ fold change vs. $-\log_{10}$(qvalue). Red indicates those genes
832 with a q-value ≤ 0.05 and a $\log_2$ fold change ≤ -0.3 or ≥ 0.3. Heat maps depicting the
833 Z-score of the $\log_2$ fold change comparing *PmiR1* to *NTmiR* for three independent
834 replicates looking at **(B)** B cell genes and **(C)** apoptosis genes. **(D)** RNAseq results for
835 RP cells treated for 48h with 300nM tazemetostat compared to vehicle control
836 (DMSO). **(E)** Overlapping genes with increased expression following *PRDM1* KD or
837 tazemetostat treatment. **(F)** Overlapping genes with decreased expression following
838 *PRDM1* KD or tazemetostat treatment. Overlaps tested using Fisher's exact test. Heat
839 maps depicting the Z-score of the $\log_2$ fold change comparing tazemetostat treatment
840 to DMSO for three independent replicates looking at **(G)** B cell genes and **(H)**
841 apoptosis genes.
842
843 **Figure 4:** BLIMP1 and EZH2 are present at a subset of proximal genomic loci
844 **(A)** Venn diagram of H3K27me3 and BLIMP1 peaks extended ±10kb, showing
845 overlaps in these regions. (ns) not significant as determined by hypergeometric test.
846 Called peaks determined by overlap from peak calling from two independent
847 experiments. **(B)** Enrichment of signal from ChIPseq tracks ±3kb from the centre of
848 BLIMP1 binding sites. Data depicts representative experiment of two biological
849 replicates. **(C)** Venn diagram of genes assigned to H3K27me3 and BLIMP1 peaks
850 showing overlapping genes. p= 2.9e-25 as determined by Fisher's exact test. **(D)**
851 ChIPseq tracks for H3K27me3 and BLIMP1 in the RP cell line. Data represents
852 combination of reads from two independent experiments. **(E)** Enrichment of signal
853 from ChIPseq tracks ±10kb from the centre of BLIMP1 binding sites in the NCI-
854 H929 cell line. **(F)** Venn diagram depicting the overlap in genes with significantly
855 increased expression following BLIMP1 KD and genes assigned to BLIMP1 binding
856 sites. p= 7e-15, as determined by Fisher's exact test. **(G)** Venn diagram depicting the
857 overlap in genes with significantly decreased expression following BLIMP1 KD and

genes assigned to BLIMP1 binding sites. (ns) not significant as determined by Fisher's exact test. **(H)** Venn diagram depicting genes with significantly increased expression following tazemetostat treatment overlapping with genes assigned to H3K27me3 peaks. p= 7.9e-9, as determined by Fisher's exact test. **(I)** Venn diagram depicting genes with significantly decreased expression following tazemetostat treatment overlapping with genes assigned to H3K27me3 peaks. (ns) not significant, as determined by Fisher's exact test. All ChIPseq experiments were performed as two biological replicates.

Figure 5: BLIMP1 and EZH2 promote immune evasion

(A) Heat maps showing z-score of the log2 fold change for *PmiR2* compared to *NTmiR* and in RP cells with three independent replicates looking at genes involved in stimulation of T and NK cells, MHC molecules, inhibitory ligands and receptors, IFN and TNF receptors and downstream signalling. ChIPseq tracks for H3K27me3 and BLIMP1 in the RP cell line over **(B)** the immune surface molecule genes *HLA-B, MICA, LILRB1, NCR3LG1, TNFRSF1A*, or **(C)** the downstream signalling genes, *IFIT2* and *STAT1*. Data represents combination of reads from two independent experiments. **(D)** Percentage CD56+CD107a+ cells (Q2) representing degranulating NK cells, as determined by flow cytometry following co-culture with RP cells with *NTmiR* or *PmiR1*, or RP cells treated with DMSO or Tazemetostat. One representative experiment is displayed. **(E)** Relative quantification of the degranulation assay **p = 0.0088. **(F)** Cytotoxicity depicted in relative luminescence units (RLU), as measured by adenylate kinase activity in the culture media following 4 h co-culture of NK cells with RP cells expressing *NTmiR* or *PmiR1*, or RP cells treated with DMSO or 1μM Tazemetostat. Cells were co-cultured at the effector:target ratio of 20:1. ****p = 3.1×10^{-5}; *p = 0.02. Results of the degranulation and cytotoxicity assays from four individual donors, performed in two pairs on two separate occasions.

Expanded view

Expanded view figure legends

Expanded view Figure 1

(A) Annexin V staining of dox-induced RP cells with *NTmiR*, *PmiR1* or *PmiR2*; ***p = 0.0004; **p = 0.0071. **(B)** Annexin V staining of dox-induced MW cells with *NTmiR* or *PmiR1*; p = 0.0572.

Expanded view Figure 2

(A) Signal intensity of immunofluorescence staining for BLIMP1 and EZH2 as quantified by CellProfiler from approximately 5000 cells per sample across two independenct replicates. **(B)** Relative growth of RP cells treated with tazemetostat for 96h, shown next to RP cells treated with Ibrutinib for 48h. **(C)** Immunoblot of histone extracts from RP cells stained for H3K27me3 with total H3 as a loading control following 48h tazemetostat treatment at the indicated concentrations. The 0 concentration was treated with vehicle control, DMSO.

Expanded view Figure 3

(A) Graph of RNAseq results depicting normalised transcripts per million (TPM) values for *SMURF2* in RP cells with *NTmiR* and *PmiR1*. Bar plots depicting normalised enrichment score for Hallmarks gene sets identified using GSEA pre-ranked with FDR-corrected p-value ≤ 0.05 for **(B)** *PmiR1* compared to *NTmiR* and **(C)** tazemetostat treatment compared to DMSO.

Expanded view Figure 4

(A) Motif enrichment analysis showing the top motif for BLIMP1 ChIPseq experiments in the RP cell line. Profiles showing enrichment over ±30 kb regions from TSSs assigned to **(B)** BLIMP1 and **(C)** H3K27me3 peaks in the RP cell line. **(D)** Motif enrichment analysis showing the top motif for BLIMP1 ChIPseq experiments in the OPM-2 and NCI-H929 cell lines. Profiles showing enrichment over ±30 kb regions from TSSs assigned to **(E)** BLIMP1, **(F)** H3K27me3 and **(G)** EZH2 peaks in the OPM-2 and NCI-H929 cell lines. **(H)** Enrichment of BLIMP1 signal in the RP, OPM-2 and NCI-H929 cell lines over BLIMP1 peaks from the RP cell line. **(I)**

Enrichment of H3K27me3 signal in the RP, OPM-2 and NCI-H929 cell lines over H3K27me3 peaks from the RP cell line. **(J)** ChIPseq tracks for H3K27me3 and BLIMP1 over the *SMURF2* gene in the RP cell line. **(K)** Venn diagrams of H3K27me3 and BLIMP1 peaks extended ±10kb, showing overlaps in these regions in the OPM-2 and NCI-H929 cell lines. (ns) not significant as determined by hypergeometric test. **(L)** Venn diagram of EZH2 and BLIMP1 peaks extended ±10kb, showing overlaps in these regions in the NCI-H929 cell line. (ns) not significant as determined by hypergeometric test. **(M)** Venn diagrams of overlapping genes assigned to peaks for H3K27me3 or BLIMP1 in the OPM-2 and NCI-H929 cell lines. Significance determined by Fisher's exact test. OPM-2, ns, not significant; NCI-H929, p = 5.9e-20. **(N)** Venn diagram of overlapping genes assigned to peaks for EZH2 or BLIMP1 in the NCI-H929 cell lines. (ns) not significant, as determined by Fisher's exact test.

Expanded view Figure 5

(A) ChIPseq tracks for H3K27me3 and BLIMP1 over the *PDCD1LG2* gene in the RP cell line. **(B)** Heat map showing the z-score of the $_{log2}$ fold change for Tazemetostat compared to DMSO in RP cells with three independent replicates looking at genes involved in stimulation of NK cells, MHC molecules, inhibitory ligands and receptors, and downstream signalling. **(C)** RT-qPCR from three independent experiments depicting relative mRNA expression comparing RP cells with *NTmiR*, and *PmiR1* transduced with EGFP or EZH2-EGFP. **(D)** Negative control for the degranulation assay, consisting of NK cells cultured alone, and positive control consisting of NK cells in co-culture with RP cells treated with 2.5µg/mL phorbol 12-myristate 13-acetate and 0.5µg/mL ionomycin.

Appendix

Appendix Methods

Resazurin assay

The percentage reduction of resazurin was calculated according to the following formula:

$$\text{Percentage reduction of resazurin} = \frac{(O2 \times A1) - (O1 \times A2)}{(R1 \times N2) - (R2 \times N1)} \times 100$$

Where O1 = molar extinction coefficient (E) of oxidized resazurin at 570 nm (80586); O2= E of oxidized resazurin at 595 nm (117216); R1 = E of reduced resazurin (Red) at 570 nm (155677); R2= E of reduced resazurin at 595 nm (14652); A1 = absorbance of test wells at 570 nm; A2 = absorbance of test wells at 595 nm; N1 = absorbance of negative control well (media plus resazurin but no cells) at 570 nm; N2 = absorbance of negative control well (media plus resazurin but no cells) at 595 nm.

Appendix Table 1: Artificial miRNA sequences

Name	Sequence (5'-3')
PmiR1	G**TACACTTCTCTTCAAACTCAG**GTTTTGGCCACTGACTGAC CTGAGTTTAGAGAAGTGTACA
PmiR2	G**TTACTCATCACTCCAATAACC**GTTTTGGCCACTGACTGAC GGTTATTGGTGATGAGTAACA
Non-targeting (*NTmiR*)	**AAATGTACTGCGCGTGGAGAC**GTTTTGGCCACTGACTGAC GTCTCCACGCAGTACATTT

Appendix Table 2: Primers used for mutagenesis

FUW-P-miR1-mut_Fwd	gaaaaatgcaCATACATTGTGAACGACCA C
FUW-P-miR1-mut_Rev	ctcgaattccgCCTCTGTCCACAGAGTCA

Appendix Table 3: Primers used for qPCR

Primer	**Sequence**

PRDM1_fwd PRDM1_rev	GGTACACACGGGAGAAAAGC GAGATTGCTGGTGCTGCTAA
EZH2_fwd EZH2_rev	ACATCCTTTTCATGCAACACC GCTCCCTCCAAATGCTGGTA
STAT1_fwd STAT1_rev	CTGTGCGTAGCTGCTCCTT GAGTCAAGCTGCTGAAGTTCG
TFEC_fwd TFEC_rev	ACATGGGGCTTACAAGTGCT TCAATGAGGTTGTGGTTGTCC
POU2F2_fwd POU2F2_rev	ACTCATGTTGACGGGCAGC GGTAGCAGGAACTGAGCAGG
MICA_fwd MICA_rev	ACATTCCATGTTTCTGCTGTTGC GACCTGCAGGCTCACGA
LGALS9_fwd LGALS9_rev	TCAATGGGACCGTTCTCAGC GAGGGTTGAAGTGGAAGGCA
BCL2L11_fwd BCL2L11_rev	CCTCGGCGCCCTTTCTT AGGTTGCTTTGCCATTTGGTC
CASP4_fwd CASP4_rev	TGCTGTTTACAAGACCCACG AGAGCCCATTGTGCTGTCTC
OAS2_fwd OAS2_rev	CAGGAACCCGAACAGTTCCC AGGACAAGGGTACCATCGGA
PIK3CD_fwd PIK3CD_rev	TGTACGCCGTGATCGAGAAA CGGTCTTAAGCTGGTCCTTGT

RCAN3_fwd RCAN3_rev	GCGCGAATAGAACTCCACGA GCGGCAGGAGATAGGACTTG
ZFP36L1_fwd ZFP36L1_rev	GTCTGCCACCATCTTCGACT TTTCTGTCCAGCAGGCAACC
CIITA_fwd CIITA_rev	CATCCTTGGGGAAGCTGAGG CTGTGAGCTGCCTTGGGG
TNFRSF14_fwd TNFRSF14_rev	GCAGTGCCAAATGTGTGACC CCTGGACGATGCAGAAGTGG
HAVCR2_fwd HAVCR2_rev	GGCTCTTATCTTCGGCGCT GGGAGGTTGGCCAAAGAGAT
PPIA_fwd PPIA_rev	CATCTGCACTGCCAAGACTGA TGGCCTCCACAATATTCATGC
ACTIN_fwd ACTIN_rev	AGGCACCAGGGCGTGAT GCCCACATAGGAATCCTTCTGAC

971

972 **References**

973 Basso K, Dalla-Favera R (2015) Germinal centres and B cell lymphomagenesis.
974 Nature Reviews Immunology 15: 172
975 Béguelin W, Popovic R, Teater M, Jiang Y, Bunting Karen L, Rosen M, Shen H,
976 Yang Shao N, Wang L, Ezponda T, Martinez-Garcia E, Zhang H, Zheng Y, Verma
977 Sharad K, McCabe Michael T, Ott Heidi M, Van Aller Glenn S, Kruger Ryan G, Liu Y,
978 McHugh Charles F et al. (2013) EZH2 Is Required for Germinal Center Formation
979 and Somatic EZH2 Mutations Promote Lymphoid Transformation. Cancer Cell
980 23: 677-692
981 Boyer LA, Lee TI, Cole MF, Johnstone SE, Levine SS, Zucker JP, Guenther MG,
982 Kumar RM, Murray HL, Jenner RG, Gifford DK, Melton DA, Jaenisch R, Young RA
983 (2005) Core Transcriptional Regulatory Circuitry in Human Embryonic Stem
984 Cells. Cell 122: 947-956
985 Bracken AP, Pasini D, Capra M, Prosperini E, Colli E, Helin K (2003) EZH2 is
986 downstream of the pRB-E2F pathway, essential for proliferation and amplified in
987 cancer. Embo j 22: 5323-35
988 Brandefors L, Melin B, Lindh J, Lundqvist K, Kimby E (2018) Prognostic factors
989 and primary treatment for Waldenström macroglobulinemia – a Swedish
990 Lymphoma Registry study. British Journal of Haematology 183: 564-577
991 Bray NL, Pimentel H, Melsted P, Pachter L (2016) Near-optimal probabilistic
992 RNA-seq quantification. Nature biotechnology 34: 525
993 Burnette WN (1981) "Western Blotting": Electrophoretic transfer of proteins
994 from sodium dodecyl sulfate-polyacrylamide gels to unmodified nitrocellulose
995 and radiographic detection with antibody and radioiodinated protein A.
996 Analytical Biochemistry 112: 195-203
997 Calado DP, Zhang B, Srinivasan L, Sasaki Y, Seagal J, Unitt C, Rodig S, Kutok J,
998 Tarakhovsky A, Schmidt-Supprian M, Rajewsky K (2010) Constitutive Canonical
999 NF-κB Activation Cooperates with Disruption of BLIMP1 in the Pathogenesis of
1000 Activated B Cell-like Diffuse Large Cell Lymphoma. Cancer Cell 18: 580-589
1001 Carpenter AE, Jones TR, Lamprecht MR, Clarke C, Kang IH, Friman O, Guertin DA,
1002 Chang JH, Lindquist RA, Moffat J, Golland P, Sabatini DM (2006) CellProfiler:
1003 image analysis software for identifying and quantifying cell phenotypes. Genome
1004 biology 7: R100
1005 Carroll D, Erhardt S, Pagani M, Barton SC, Surani MA, Jenuwein T (2001) The
1006 Polycomb-Group Gene Ezh2 Is Required for Early Mouse Development.
1007 Molecular and Cellular Biology 21: 4330
1008 Chen H, Gilbert CA, Hudson JA, Bolick SC, Wright KL, Piskurich JF (2007) Positive
1009 regulatory domain I-binding factor 1 mediates repression of the MHC class II
1010 transactivator (CIITA) type IV promoter. Molecular Immunology 44: 1461-1470
1011 Croonquist PA, Van Ness B (2005) The polycomb group protein enhancer of
1012 zeste homolog 2 (EZH2) is an oncogene that influences myeloma cell growth and
1013 the mutant ras phenotype. Oncogene 24: 6269
1014 Czermin B, Melfi R, McCabe D, Seitz V, Imhof A, Pirrotta V (2002) Drosophila
1015 Enhancer of Zeste/ESC Complexes Have a Histone H3 Methyltransferase Activity
1016 that Marks Chromosomal Polycomb Sites. Cell 111: 185-196
1017 de Charette M, Houot R (2018) Hide or defend, the two strategies of lymphoma
1018 immune evasion: potential implications for immunotherapy. Haematologica 103:
1019 1256-1268

1020 Doody GM, Stephenson S, McManamy C, Tooze RM (2007) PRDM1/BLIMP-1
1021 Modulates IFN-γ-Dependent Control of the MHC Class I Antigen-Processing and
1022 Peptide-Loading Pathway. The Journal of Immunology 179: 7614
1023 Elias S, Robertson EJ, Bikoff EK, Mould AW (2018a) Blimp-1/PRDM1 is a critical
1024 regulator of Type III Interferon responses in mammary epithelial cells. Scientific
1025 reports 8: 237-237
1026 Elias S, Robertson EJ, Bikoff EK, Mould AW (2018b) Blimp-1/PRDM1 is a critical
1027 regulator of Type III Interferon responses in mammary epithelial cells. Scientific
1028 Reports 8: 237
1029 Gavriatopoulou M, Musto P, Caers J, Merlini G, Kastritis E, van de Donk N, Gay F,
1030 Hegenbart U, Hajek R, Zweegman S, Bruno B, Straka C, Dimopoulos MA, Einsele
1031 H, Boccadoro M, Sonneveld P, Engelhardt M, Terpos E (2018) European myeloma
1032 network recommendations on diagnosis and management of patients with rare
1033 plasma cell dyscrasias. Leukemia 32: 1883-1898
1034 Gertz MA (2019) Waldenström macroglobulinemia: 2019 update on diagnosis,
1035 risk stratification, and management. American Journal of Hematology 94: 266-
1036 276
1037 Guo M, Price MJ, Patterson DG, Barwick BG, Haines RR, Kania AK, Bradley JE,
1038 Randall TD, Boss JM, Scharer CD (2018) EZH2 Represses the B Cell
1039 Transcriptional Program and Regulates Antibody-Secreting Cell Metabolism and
1040 Antibody Production. The Journal of Immunology 200: 1039-1052
1041 Győry I, Wu J, Fejér G, Seto E, Wright KL (2004) PRDI-BF1 recruits the histone H3
1042 methyltransferase G9a in transcriptional silencing. Nature Immunology 5: 299
1043 Hackett JA, Sengupta R, Zylicz JJ, Murakami K, Lee C, Down TA, Surani MA (2013)
1044 Germline DNA demethylation dynamics and imprint erasure through 5-
1045 hydroxymethylcytosine. Science (New York, NY) 339: 448-452
1046 Hernando H, Gelato KA, Lesche R, Beckmann G, Koehr S, Otto S, Steigemann P,
1047 Stresemann C (2016) EZH2 Inhibition Blocks Multiple Myeloma Cell Growth
1048 through Upregulation of Epithelial Tumor Suppressor Genes. Molecular Cancer
1049 Therapeutics 15: 287
1050 Hou B, Saudan P, Ott G, Wheeler Matthew L, Ji M, Kuzmich L, Lee Linda M,
1051 Coffman Robert L, Bachmann Martin F, DeFranco Anthony L (2011) Selective
1052 Utilization of Toll-like Receptor and MyD88 Signaling in B Cells for Enhancement
1053 of the Antiviral Germinal Center Response. Immunity 34: 375-384
1054 Hung KH, Su ST, Chen CY, Hsu PH, Huang SY, Wu WJ, Chen MJM, Chen HY, Wu PC,
1055 Lin FR, Tsai MD, Lin KI (2016) Aiolos collaborates with Blimp-1 to regulate the
1056 survival of multiple myeloma cells. Cell Death And Differentiation 23: 1175
1057 Hunter ZR, Xu L, Yang G, Tsakmaklis N, Vos JM, Liu X, Chen J, Manning RJ, Chen JG,
1058 Brodsky P, Patterson CJ, Gustine J, Dubeau T, Castillo JJ, Anderson KC, Munshi
1059 NM, Treon SP (2016) Transcriptome sequencing reveals a profile that
1060 corresponds to genomic variants in Waldenström macroglobulinemia. Blood
1061 128: 827-838
1062 Iwanaga M, Chiang CJ, Soda M, Lai MS, Yang YW, Miyazaki Y, Matsuo K, Matsuda
1063 T, Sobue T (2014) Incidence of lymphoplasmacytic lymphoma/Waldenstrom's
1064 macroglobulinaemia in Japan and Taiwan population-based cancer registries,
1065 1996-2003. International journal of cancer 134: 174-80
1066 Jalali S, Price-Troska T, Paludo J, Villasboas J, Kim H-J, Yang Z-Z, Novak AJ, Ansell
1067 SM (2018) Soluble PD-1 ligands regulate T-cell function in Waldenstrom
1068 macroglobulinemia. Blood Advances 2: 1985

1069 Kallies A, Hasbold J, Tarlinton DM, Dietrich W, Corcoran LM, Hodgkin PD, Nutt SL
1070 (2004) Plasma Cell Ontogeny Defined by Quantitative Changes in Blimp-1
1071 Expression. The Journal of Experimental Medicine 200: 967
1072 Kent WJ, Sugnet CW, Furey TS, Roskin KM, Pringle TH, Zahler AM, Haussler,
1073 David (2002) The Human Genome Browser at UCSC. Genome Research 12: 996-
1074 1006
1075 Kim KH, Roberts CWM (2016) Targeting EZH2 in cancer. Nature Medicine 22:
1076 128
1077 Kleer CG, Cao Q, Varambally S, Shen R, Ota I, Tomlins SA, Ghosh D, Sewalt RGAB,
1078 Otte AP, Hayes DF, Sabel MS, Livant D, Weiss SJ, Rubin MA, Chinnaiyan AM
1079 (2003) EZH2 is a marker of aggressive breast cancer and promotes neoplastic
1080 transformation of breast epithelial cells. Proceedings of the National Academy of
1081 Sciences 100: 11606
1082 Kuo TC, Calame KL (2004) B Lymphocyte-Induced Maturation Protein (Blimp)-1,
1083 IFN Regulatory Factor (IRF)-1, and IRF-2 Can Bind to the Same Regulatory Sites.
1084 The Journal of Immunology 173: 5556
1085 Kurimoto K, Yabuta Y, Hayashi K, Ohta H, Kiyonari H, Mitani T, Moritoki Y, Kohri
1086 K, Kimura H, Yamamoto T, Katou Y, Shirahige K, Saitou M (2015) Quantitative
1087 Dynamics of Chromatin Remodeling during Germ Cell Specification from Mouse
1088 Embryonic Stem Cells. Cell Stem Cell 16: 517-532
1089 Kyle RA, Larson DR, McPhail ED, Therneau TM, Dispenzieri A, Kumar S, Kapoor P,
1090 Cerhan JR, Rajkumar SV (2018) Fifty-Year Incidence of Waldenstrom
1091 Macroglobulinemia in Olmsted County, Minnesota, From 1961 Through 2010: A
1092 Population-Based Study With Complete Case Capture and Hematopathologic
1093 Review. Mayo Clinic proceedings 93: 739-746
1094 Langmead B, Salzberg SL (2012) Fast gapped-read alignment with Bowtie 2.
1095 Nature Methods 9: 357
1096 Lawrence DW, Kornbluth J (2016) E3 ubiquitin ligase NKLAM ubiquitinates
1097 STAT1 and positively regulates STAT1-mediated transcriptional activity. Cellular
1098 Signalling 28: 1833-1841
1099 Liberzon A, Birger C, Thorvaldsdottir H, Ghandi M, Mesirov JP, Tamayo P (2015)
1100 The Molecular Signatures Database (MSigDB) hallmark gene set collection. Cell
1101 systems 1: 417-425
1102 Lin F-R, Kuo H-K, Ying H-Y, Yang F-H, Lin K-I (2007) Induction of Apoptosis in
1103 Plasma Cells by B Lymphocyte–Induced Maturation Protein-1 Knockdown.
1104 Cancer Research 67: 11914
1105 Lin K-I, Angelin-Duclos C, Kuo TC, Calame K (2002) Blimp-1-dependent
1106 repression of Pax-5 is required for differentiation of B cells to immunoglobulin
1107 M-secreting plasma cells. Molecular and cellular biology 22: 4771-4780
1108 Lin Y, Wong K-k, Calame K (1997) Repression of c-myc transcription by Blimp-1,
1109 an inducer of terminal B cell differentiation. Science 276: 596-599
1110 Lois C, Hong EJ, Pease S, Brown EJ, Baltimore D (2002) Germline transmission
1111 and tissue-specific expression of transgenes delivered by lentiviral vectors.
1112 Science 295: 868-872
1113 Magnúsdóttir E, Dietmann S, Murakami K, Günesdogan U, Tang F, Bao S,
1114 Diamanti E, Lao K, Gottgens B, Azim Surani M (2013) A tripartite transcription
1115 factor network regulates primordial germ cell specification in mice. Nature Cell
1116 Biology 15: 905

1117 Magnúsdóttir E, Kalachikov S, Mizukoshi K, Savitsky D, Ishida-Yamamoto A,
1118 Panteleyev AA, Calame K (2007) Epidermal terminal differentiation depends on
1119 B lymphocyte-induced maturation protein-1. Proceedings of the National
1120 Academy of Sciences 104: 14988
1121 Mandelbaum J, Bhagat G, Tang H, Mo T, Brahmachary M, Shen Q, Chadburn A,
1122 Rajewsky K, Tarakhovsky A, Pasqualucci L, Dalla-Favera R (2010) BLIMP1 is a
1123 Tumor Suppressor Gene Frequently Disrupted in Activated B Cell-like Diffuse
1124 Large B Cell Lymphoma. Cancer cell 18: 568-579
1125 Martins G, Calame K (2008) Regulation and Functions of Blimp-1 in T and B
1126 Lymphocytes. Annual Review of Immunology 26: 133-169
1127 Minnich M, Tagoh H, Bönelt P, Axelsson E, Fischer M, Cebolla B, Tarakhovsky A,
1128 Nutt SL, Jaritz M, Busslinger M (2016) Multifunctional role of the transcription
1129 factor Blimp-1 in coordinating plasma cell differentiation. Nature Immunology
1130 17: 331
1131 Morgan MAJ, Magnusdottir E, Kuo TC, Tunyaplin C, Harper J, Arnold SJ, Calame K,
1132 Robertson EJ, Bikoff EK (2009) Blimp-1/Prdm1 Alternative Promoter Usage
1133 during Mouse Development and Plasma Cell Differentiation. Molecular and
1134 Cellular Biology 29: 5813
1135 Morin RD, Johnson NA, Severson TM, Mungall AJ, An J, Goya R, Paul JE, Boyle M,
1136 Woolcock BW, Kuchenbauer F, Yap D, Humphries RK, Griffith OL, Shah S, Zhu H,
1137 Kimbara M, Shashkin P, Charlot JF, Tcherpakov M, Corbett R et al. (2010) Somatic
1138 mutations altering EZH2 (Tyr641) in follicular and diffuse large B-cell
1139 lymphomas of germinal-center origin. Nature Genetics 42: 181
1140 Mould AW, Morgan MAJ, Nelson AC, Bikoff EK, Robertson EJ (2015)
1141 Blimp1/Prdm1 Functions in Opposition to Irf1 to Maintain Neonatal Tolerance
1142 during Postnatal Intestinal Maturation. PLOS Genetics 11: e1005375
1143 Müller J, Hart CM, Francis NJ, Vargas ML, Sengupta A, Wild B, Miller EL, O'Connor
1144 MB, Kingston RE, Simon JA (2002) Histone Methyltransferase Activity of a
1145 Drosophila Polycomb Group Repressor Complex. Cell 111: 197-208
1146 Murakami K, Günesdogan U, Zylicz JJ, Tang WWC, Sengupta R, Kobayashi T, Kim
1147 S, Butler R, Dietmann S, Azim Surani M (2016) NANOG alone induces germ cells
1148 in primed epiblast in vitro by activation of enhancers. Nature 529: 403
1149 Nutt SL, Fairfax KA, Kallies A (2007) BLIMP1 guides the fate of effector B and T
1150 cells. Nature Reviews Immunology 7: 923
1151 Ohinata Y, Payer B, O'carroll D, Ancelin K, Ono Y, Sano M, Barton SC, Obukhanych
1152 T, Nussenzweig M, Tarakhovsky A (2005) Blimp1 is a critical determinant of the
1153 germ cell lineage in mice. Nature 436: 207
1154 Pardoll DM (2012) The blockade of immune checkpoints in cancer
1155 immunotherapy. Nature Reviews Cancer 12: 252
1156 Pasare C, Medzhitov R (2005) Control of B-cell responses by Toll-like receptors.
1157 Nature 438: 364
1158 Pasqualucci L, Compagno M, Houldsworth J, Monti S, Grunn A, Nandula SV, Aster
1159 JC, Murty VV, Shipp MA, Dalla-Favera R (2006) Inactivation of the
1160 PRDM1/BLIMP1 gene in diffuse large B cell lymphoma. The Journal of
1161 Experimental Medicine 203: 311
1162 Pfaffl MW (2001) A new mathematical model for relative quantification in real-
1163 time RT–PCR. Nucleic Acids Research 29: e45-e45
1164 Pimentel H, Bray NL, Puente S, Melsted P, Pachter L (2017) Differential analysis
1165 of RNA-seq incorporating quantification uncertainty. Nature methods 14: 687

1166 Piskurich JF, Lin K-I, Lin Y, Wang Y, Ting JP-Y, Calame K (2000a) BLIMP-1
1167 mediates extinction of major histocompatibility class II transactivator expression
1168 in plasma cells. Nature immunology 1: 526
1169 Piskurich JF, Lin KI, Lin Y, Wang Y, Ting JPY, Calame K (2000b) BLIMP-1 mediates
1170 extinction of major histocompatibility class II transactivator expression in
1171 plasma cells. Nature Immunology 1: 526
1172 Ramírez F, Ryan DP, Grüning B, Bhardwaj V, Kilpert F, Richter AS, Heyne S,
1173 Dündar F, Manke T (2016) deepTools2: a next generation web server for deep-
1174 sequencing data analysis. Nucleic Acids Research 44: W160-W165
1175 Ren B, Chee KJ, Kim TH, Maniatis T (1999) PRDI-BF1/Blimp-1 repression is
1176 mediated by corepressors of the Groucho family of proteins. Genes &
1177 Development 13: 125-137
1178 Roberts MJ, Chadburn A, Ma S, Hyjek E, Peterson LC (2013) Nuclear Protein
1179 Dysregulation in Lymphoplasmacytic Lymphoma/Waldenström
1180 Macroglobulinemia. American Journal of Clinical Pathology 139: 210-219
1181 Roccaro AM, Sacco A, Jia X, Azab AK, Maiso P, Ngo HT, Azab F, Runnels J, Quang P,
1182 Ghobrial IM (2010) microRNA-dependent modulation of histone acetylation in
1183 Waldenstrom macroglobulinemia. Blood: blood-2010-01-265686
1184 Savitsky D, Calame K (2006) B-1 B lymphocytes require Blimp-1 for
1185 immunoglobulin secretion. The Journal of Experimental Medicine 203: 2305
1186 Schop RFJ, Kuehl WM, Van Wier SA, Ahmann GJ, Price-Troska T, Bailey RJ, Jalal
1187 SM, Qi Y, Kyle RA, Greipp PR, Fonseca R (2002) Waldenström macroglobulinemia
1188 neoplastic cells lack immunoglobulin heavy chain locus translocations but have
1189 frequent 6q deletions. Blood 100: 2996
1190 Shaffer AL, Emre NCT, Lamy L, Ngo VN, Wright G, Xiao W, Powell J, Dave S, Yu X,
1191 Zhao H, Zeng Y, Chen B, Epstein J, Staudt LM (2008) IRF4 addiction in multiple
1192 myeloma. Nature 454: 226
1193 Shaffer AL, Lin K-I, Kuo TC, Yu X, Hurt EM, Rosenwald A, Giltnane JM, Yang L,
1194 Zhao H, Calame K, Staudt LM (2002) Blimp-1 Orchestrates Plasma Cell
1195 Differentiation by Extinguishing the Mature B Cell Gene Expression Program.
1196 Immunity 17: 51-62
1197 Shapiro-Shelef M, Lin K-I, McHeyzer-Williams LJ, Liao J, McHeyzer-Williams MG,
1198 Calame K (2003) Blimp-1 is required for the formation of immunoglobulin
1199 secreting plasma cells and pre-plasma memory B cells. Immunity 19: 607-620
1200 Shapiro-Shelef M, Lin K-I, Savitsky D, Liao J, Calame K (2005) Blimp-1 is required
1201 for maintenance of long-lived plasma cells in the bone marrow. The Journal of
1202 Experimental Medicine 202: 1471
1203 Subramanian A, Tamayo P, Mootha VK, Mukherjee S, Ebert BL, Gillette MA,
1204 Paulovich A, Pomeroy SL, Golub TR, Lander ES, Mesirov JP (2005) Gene set
1205 enrichment analysis: A knowledge-based approach for interpreting genome-
1206 wide expression profiles. Proceedings of the National Academy of Sciences 102:
1207 15545
1208 Tellier J, Shi W, Minnich M, Liao Y, Crawford S, Smyth GK, Kallies A, Busslinger M,
1209 Nutt SL (2016) Blimp-1 controls plasma cell function through the regulation of
1210 immunoglobulin secretion and the unfolded protein response. Nature
1211 Immunology 17: 323
1212 Thibult M-L, Mamessier E, Gertner-Dardenne J, Pastor S, Just-Landi S, Xerri L,
1213 Chetaille B, Olive D (2013) PD-1 is a novel regulator of human B-cell activation.
1214 International immunology 25: 129-137

1215 Tooze RM, Stephenson S, Doody GM (2006) Repression of IFN-γ Induction of
1216 Class II Transactivator: A Role for PRDM1/Blimp-1 in Regulation of Cytokine
1217 Signaling. The Journal of Immunology 177: 4584-4593
1218 Treon SP (2009) How I treat Waldenström macroglobulinemia. Blood 114: 2375
1219 Treon SP, Cao Y, Xu L, Yang G, Liu X, Hunter ZR (2014) Somatic mutations in
1220 MYD88 and CXCR4 are determinants of clinical presentation and overall survival
1221 in Waldenström macroglobulinemia. Blood 123: 2791
1222 Treon SP, Tripsas CK, Meid K, Warren D, Varma G, Green R, Argyropoulos KV,
1223 Yang G, Cao Y, Xu L, Patterson CJ, Rodig S, Zehnder JL, Aster JC, Harris NL, Kanan
1224 S, Ghobrial I, Castillo JJ, Laubach JP, Hunter ZR et al. (2015) Ibrutinib in
1225 Previously Treated Waldenström's Macroglobulinemia. New England Journal of
1226 Medicine 372: 1430-1440
1227 Treon SP, Xu L, Yang G, Zhou Y, Liu X, Cao Y, Sheehy P, Manning RJ, Patterson CJ,
1228 Tripsas C, Arcaini L, Pinkus GS, Rodig SJ, Sohani AR, Harris NL, Laramie JM,
1229 Skifter DA, Lincoln SE, Hunter ZR (2012) MYD88 L265P Somatic Mutation in
1230 Waldenström's Macroglobulinemia. New England Journal of Medicine 367: 826-
1231 833
1232 Vijay A, Gertz MA (2007) Waldenström macroglobulinemia. Blood 109: 5096-
1233 5103
1234 Vincent SD, Dunn NR, Sciammas R, Shapiro-Shalef M, Davis MM, Calame K, Bikoff
1235 EK, Robertson EJ (2005) The zinc finger transcriptional repressor
1236 Blimp1/Prdm1 is dispensable for early axis formation but is required for
1237 specification of primordial germ cells in the mouse. Development 132: 1315
1238 Vivier E, Tomasello E, Baratin M, Walzer T, Ugolini S (2008) Functions of natural
1239 killer cells. Nature Immunology 9: 503
1240 Wang H, Chen Y, Li F, Delasalle K, Wang J, Alexanian R, Kwak L, Rustveld L, Du XL,
1241 Wang M (2012) Temporal and geographic variations of Waldenstrom
1242 macroglobulinemia incidence: a large population-based study. Cancer 118: 3793-
1243 800
1244 Wu ZL, Zheng SS, Li ZM, Qiao YY, Aau MY, Yu Q (2009) Polycomb protein EZH2
1245 regulates E2F1-dependent apoptosis through epigenetically modulating Bim
1246 expression. Cell Death And Differentiation 17: 801
1247 Xu L, Hunter ZR, Yang G, Cao Y, Liu X, Manning R, Tripsas C, Chen J, Patterson CJ,
1248 Kluk M, Kanan S, Castillo J, Lindeman N, Treon SP (2014) Detection of MYD88
1249 L265P in peripheral blood of patients with Waldenström's Macroglobulinemia
1250 and IgM monoclonal gammopathy of undetermined significance. Leukemia 28:
1251 1698
1252 Yu J, Angelin-Duclos C, Greenwood J, Liao J, Calame K (2000) Transcriptional
1253 Repression by Blimp-1 (PRDI-BF1) Involves Recruitment of Histone Deacetylase.
1254 Molecular and Cellular Biology 20: 2592-2603
1255 Yu X, Li W, Deng Q, Li L, Hsi ED, Young KH, Zhang M, Li Y (2018) MYD88 L265P
1256 Mutation in Lymphoid Malignancies. Cancer Research
1257 Yu YL, Chou RH, Shyu WC, Hsieh SC, Wu CS, Chiang SY, Chang WJ, Chen JN, Tseng
1258 YJ, Lin YH, Lee W, Yeh SP, Hsu JL, Yang CC, Hung SC, Hung MC (2013) Smurf2 -
1259 mediated degradation of EZH2 enhances neuron differentiation and improves
1260 functional recovery after ischaemic stroke. EMBO Molecular Medicine 5: 531
1261 Zhan F, Tian E, Bumm K, Smith R, Barlogie B, Shaughnessy J (2003) Gene
1262 expression profiling of human plasma cell differentiation and classification of

1263 multiple myeloma based on similarities to distinct stages of late-stage B-cell
1264 development. Blood 101: 1128
1265 Zhang Y, Liu T, Meyer CA, Eeckhoute J, Johnson DS, Bernstein BE, Nusbaum C,
1266 Myers RM, Brown M, Li W, Liu XS (2008) Model-based analysis of ChIP-Seq
1267 (MACS). Genome biology 9: R137
1268 Zhou Y, Liu X, Xu L, Hunter ZR, Cao Y, Yang G, Carrasco R, Treon SP (2014)
1269 Transcriptional repression of plasma cell differentiation is orchestrated by
1270 aberrant over-expression of the ETS factor SPIB in Waldenström
1271 macroglobulinaemia. British Journal of Haematology 166: 677-689
1272 Zhu LJ, Gazin C, Lawson ND, Pages H, Lin SM, Lapointe DS, Green MR (2010)
1273 ChIPpeakAnno: a Bioconductor package to annotate ChIP-seq and ChIP-chip
1274 data. BMC bioinformatics 11: 237
1275 Zingg D, Arenas-Ramirez N, Sahin D, Rosalia RA, Antunes AT, Haeusel J, Sommer
1276 L, Boyman O (2017) The Histone Methyltransferase Ezh2 Controls Mechanisms
1277 of Adaptive Resistance to Tumor Immunotherapy. Cell Reports 20: 854-867
1278

Figure 1

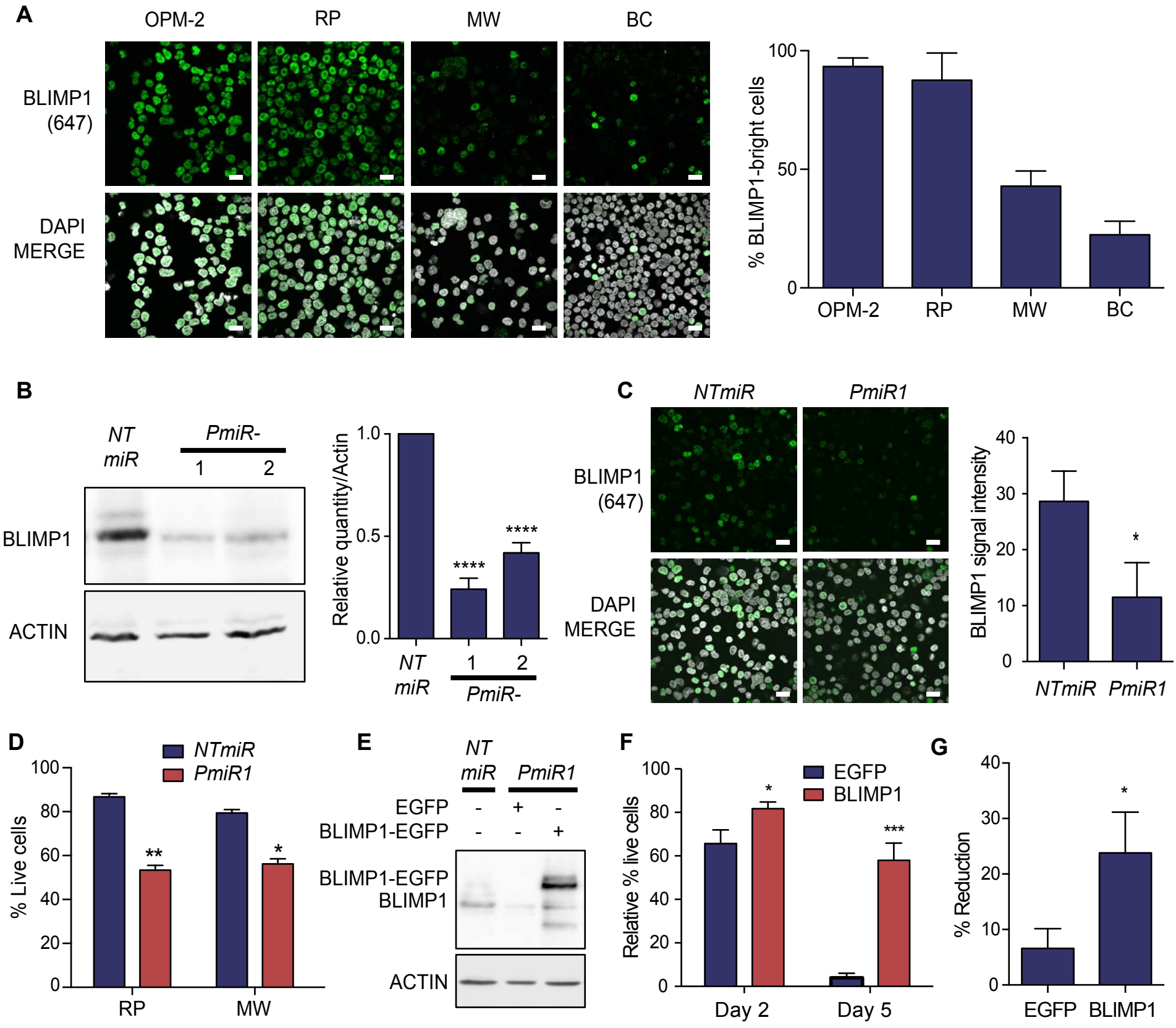

Figure 1: BLIMP1 promotes survival of WM cells

(A) BLIMP1 expression in myeloma cell line OPM-2 and in WM cell lines RP, MW and BC as detected by immunofluorescence staining, with bar graph representing percentage of BLIMP1bright cells. Scale bars represent 20μm. (B) Immunoblot of BLIMP1 expression following 48h dox induction of RP cells expressing NTmiR, PmiR1 or PmiR2, with bar graph representing the quantity of BLIMP1 relative to actin; ****$p < 0.0001$. (C) Immunofluorescence staining of BLIMP1 following 48h dox induction in MW cells expressing NTmiR, PmiR1 or PmiR2, with cell profiler quantification; $p = 0.0228$. (D) Percentage of live cells as determined by Trypan blue exclusion assay in the RP and MW cell lines. RP, $p = 0.0019$; MW, $p = 0.0162$. (E) Immunoblot depicting lentiviral ectopic expression of EGFP or BLIMP1-EGFP in the RP PmiR1 cells, next to the RP NTmiR cells. (F) The percentage of live RP PmiR1 cells with ectopic EGFP or BLIMP1-EGFP expression determined by the Trypan blue exclusion assay normalised to the percentage of live cells following transduction of RP NTmiR cells with EGFP or BLIMP1-EGFP. Day 2, *$p = 0.0165$; Day 5, ***$p = 0.0003$. (G) Per cent reduction as measured by resazurin assay for RP PmiR1 cells with EGFP or BLIMP1-EGFP, five days after dox induction. *$p = 0.0208$. All p-values as determined by student's two-tailed t-test. All graphs plotted as mean of three independent experiments, with error bars representing standard deviation.

Figure 2

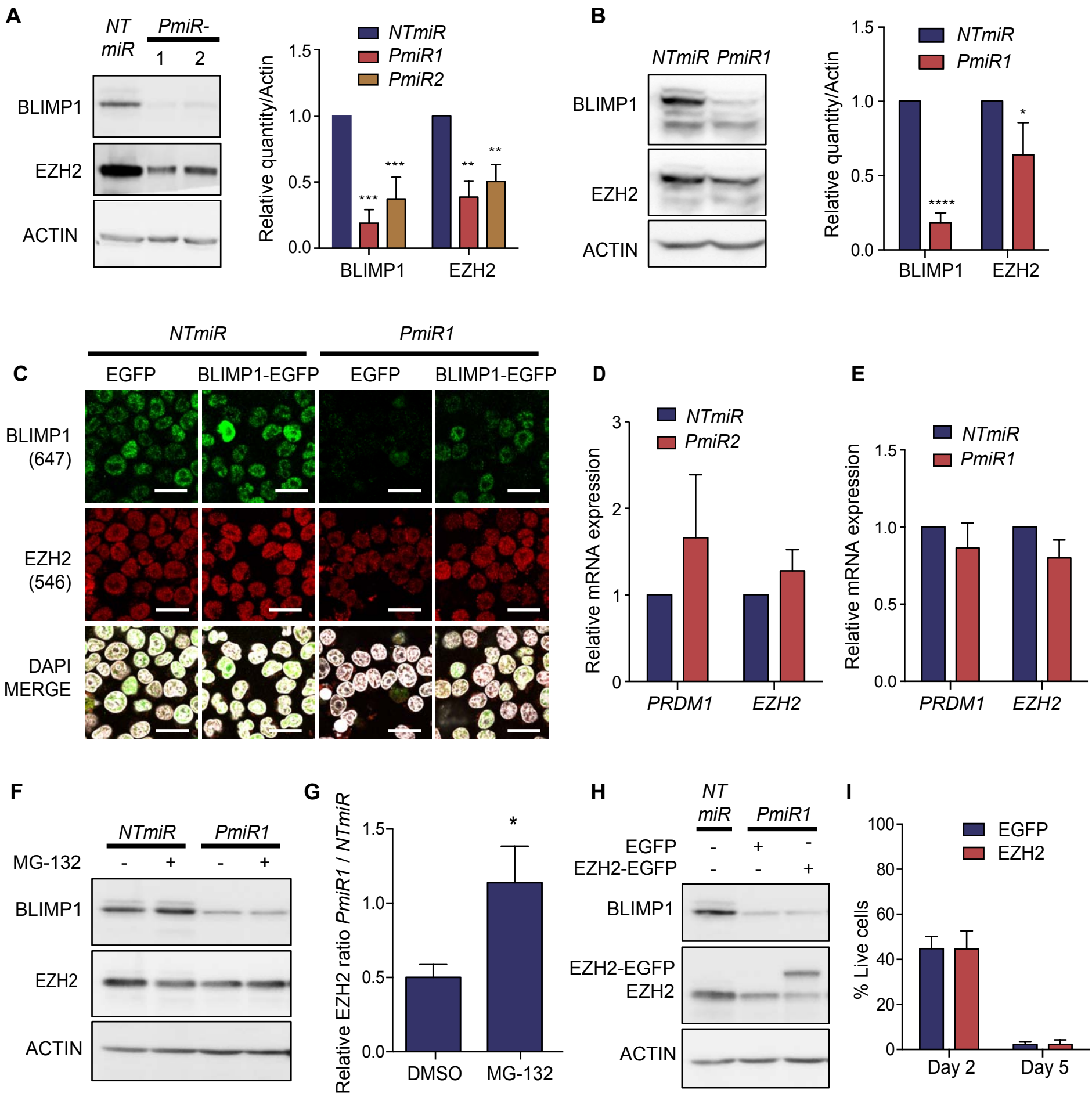

Figure 2: BLIMP1 maintains EZH2 protein levels

(A) Immunoblot of BLIMP1 and EZH2 expression following 48h dox-induction of RP cells expressing NTmiR, PmiR1 or PmiR2, with quantification of signal relative to actin in bar plot; ***p = 0.0002; ***p = 0.001; **p = 0.0027. (B) Immunoblot of BLIMP1 and EZH2 expression following 48h dox-induction of OPM-2 cells expressing NTmiR or PmiR1, with quantification of signal relative to actin in bar plot; ****p < 0.0001; *p = 0.016. (C) Immunofluorescence staining of BLIMP1 and EZH2 expression following 48 h dox-induction of RPCI-WM1 cells expressing NTmiR or PmiR1, transduced with EGFP or BLIMP1-EGFP. Scale bars represent 20 µm. (D) RT-qPCR results depicting relative mRNA expression of PRDM1 and EZH2 normalised to PPIA and ACTB in the RP cell line and (E) in the OPM-2 cell line. (F) Immunoblot of BLIMP1 and EZH2 expression following 24h dox-induction of RP cells expressing NTmiR or PmiR1 treated with DMSO or 5µM MG-132 for 4h. (G) The ratio of EZH2 expression relative to actin for RP PmiR1 cells divided by RP NTmiR cells treated with DMSO or MG132 as in Fig. 2F; p = 0.0134. (H) Immunoblot of BLIMP1 and EZH2 expression following 48h dox-induction of RP NTmiR cells or PmiR1 cells transduced with EGFP or EZH2-EGFP. (I) Percentage of live cells as determined by Trypan blue exclusion assay in the RP PmiR1 cells transduced with EGFP or EZH2-EGFP. All p-values as determined by student's two-tailed t-test. All graphs plotted as mean of three independent experiments with error bars representing standard deviation.

Figure 3

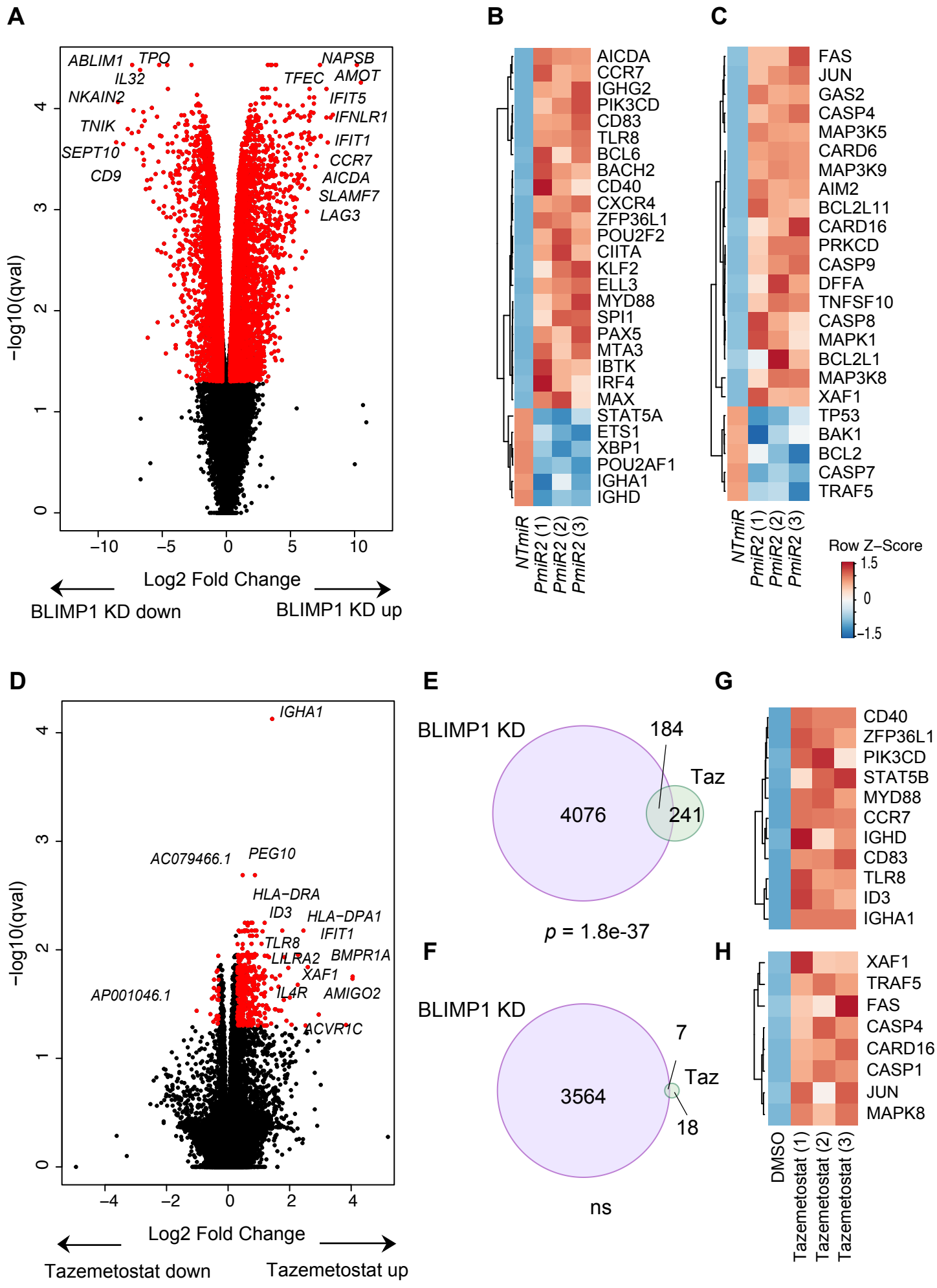

Figure 3: BLIMP1 KD induces large transcriptional changes

RNAseq results for (A) 48h dox-induced RP cells comparing PmiR1 to NTmiR. Values are plotted as log2 fold change vs. –log10(qvalue). Red indicates those genes with a q-value ≤ 0.05 and a log2 fold change ≤ -0.3 or ≥ 0.3. Heat maps depicting the Z-score of the log2 fold change comparing PmiR1 to NTmiR for three independent replicates looking at (B) B cell genes and (C) apoptosis genes. (D) RNAseq results for RP cells treated for 48h with 300nM tazemetostat compared to vehicle control (DMSO). (E) Overlapping genes with increased expression following PRDM1 KD or tazemetostat treatment. (F) Overlapping genes with decreased expression following PRDM1 KD or tazemetostat treatment. Overlaps tested using Fisher's exact test. Heat maps depicting the Z-score of the log2 fold change comparing tazemetostat treatment to DMSO for three independent replicates looking at (G) B cell genes and (H) apoptosis genes.

Figure 4

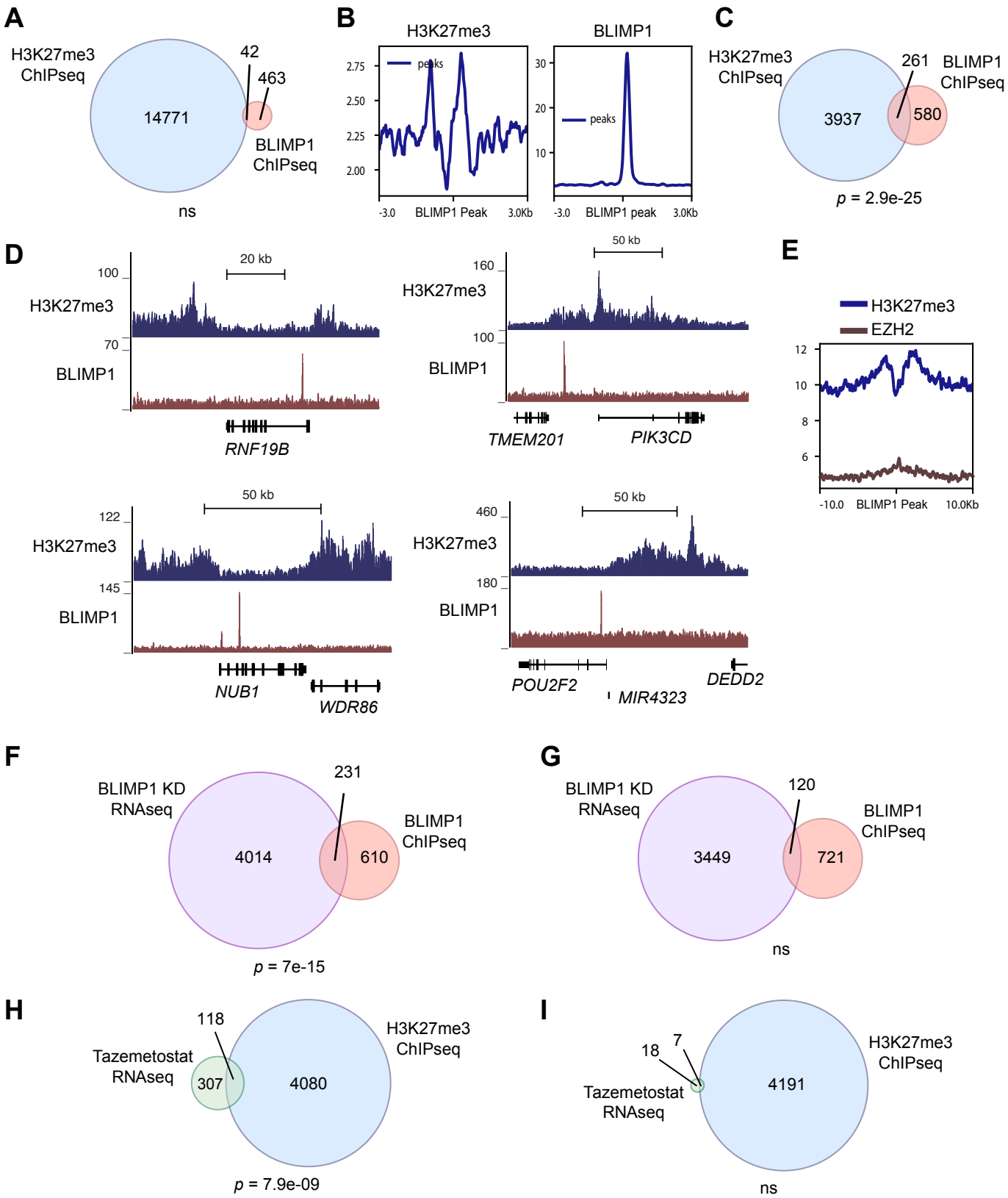

Figure 4: BLIMP1 and EZH2 are present at a subset of proximal genomic loci

(A) Venn diagram of H3K27me3 and BLIMP1 peaks extended ±10kb, showing overlaps in these regions. (ns) not significant as determined by hypergeometric test. Called peaks determined by overlap from peak calling from two independent experiments. (B) Enrichment of signal from ChIPseq tracks ±3kb from the centre of BLIMP1 binding sites. Data depicts representative experiment of two biological replicates. (C) Venn diagram of genes assigned to H3K27me3 and BLIMP1 peaks showing overlapping genes. p= 2.9e-25 as determined by Fisher's exact test. (D) ChIPseq tracks for H3K27me3 and BLIMP1 in the RP cell line. Data represents combination of reads from two independent experiments. (E) Enrichment of signal from ChIPseq tracks ±10kb from the centre of BLIMP1 binding sites in the NCI-H929 cell line. (F) Venn diagram depicting the overlap in genes with significantly increased expression following BLIMP1 KD and genes assigned to BLIMP1 binding sites. p= 7e-15, as determined by Fisher's exact test. (G) Venn diagram depicting the overlap in genes with significantly decreased expression following BLIMP1 KD and genes assigned to BLIMP1 binding sites. (ns) not significant as determined by Fisher's exact test. (H) Venn diagram depicting genes with significantly increased expression following tazemetostat treatment overlapping with genes assigned to H3K27me3 peaks. p= 7.9e-9, as determined by Fisher's exact test. (I) Venn diagram depicting genes with significantly decreased expression following tazemetostat treatment overlapping with genes assigned to H3K27me3 peaks. (ns) not significant, as determined by Fisher's exact test. All ChIPseq experiments were performed as two biological replicates.

Figure 5

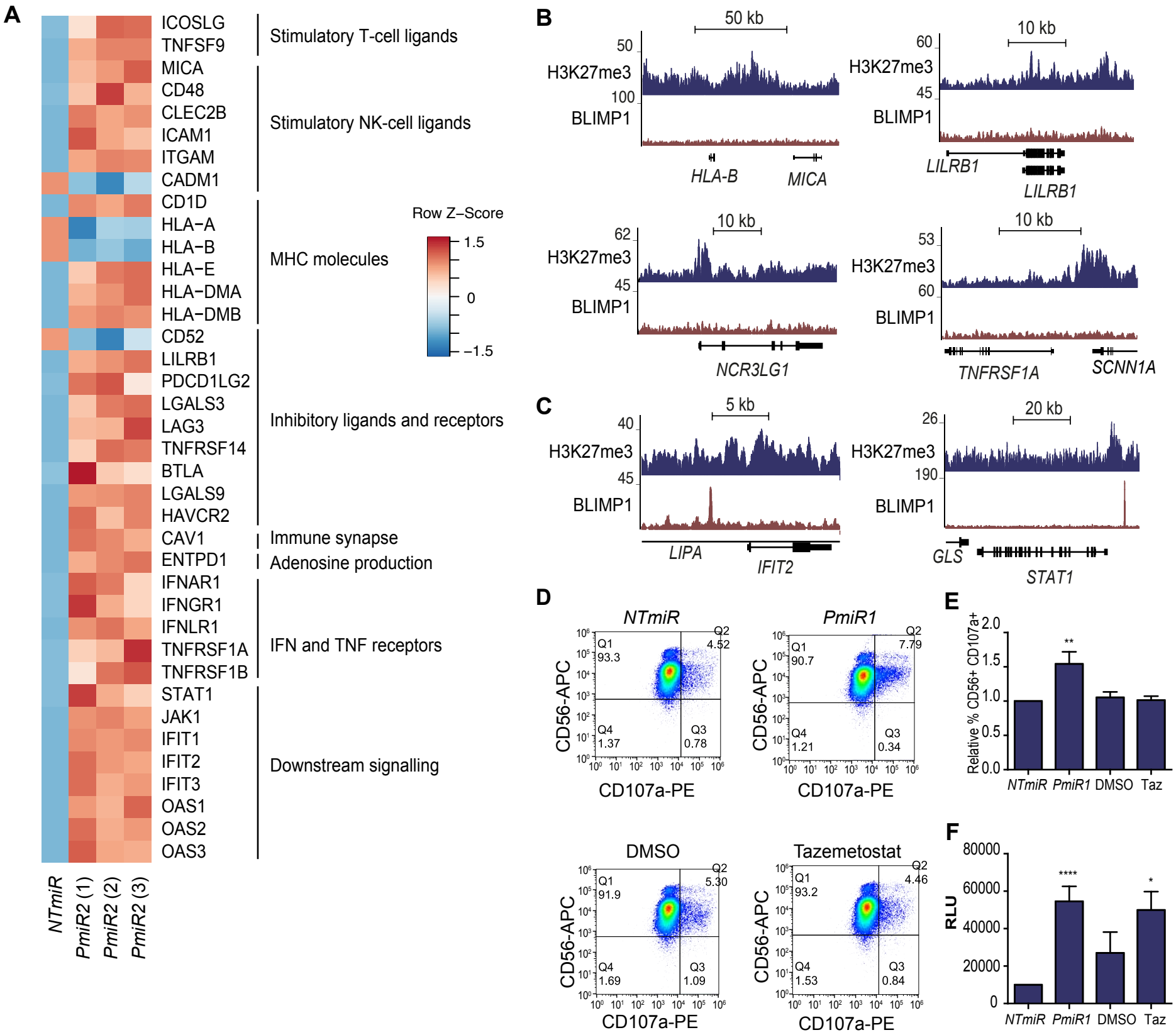

Figure 5: BLIMP1 and EZH2 promote immune evasion

(A) Heat maps showing z-score of the log2 fold change for PmiR2 compared to NTmiR and in RP cells with three independent replicates looking at genes involved in stimulation of T and NK cells, MHC molecules, inhibitory ligands and receptors, IFN and TNF receptors and downstream signalling. ChIPseq tracks for H3K27me3 and BLIMP1 in the RP cell line over (B) the immune surface molecule genes HLA-B, MICA, LILRB1, NCR3LG1, TNFRSF1A, or (C) the downstream signalling genes, IFIT2 and STAT1. Data represents combination of reads from two independent experiments. (D) Percentage CD56+CD107a+ cells (Q2) representing degranulating NK cells, as determined by flow cytometry following co-culture with RP cells with NTmiR or PmiR1, or RP cells treated with DMSO or Tazemetostat. One representative experiment is displayed. (E) Relative quantification of the degranulation assay **p = 0.0088. (F) Cytotoxicity depicted in relative luminescence units (RLU), as measured by adenylate kinase activity in the culture media following 4 h co-culture of NK cells with RP cells expressing NTmiR or PmiR1, or RP cells treated with DMSO or 1μM Tazemetostat. Cells were co-cultured at the effector:target ratio of 20:1. ****p = 3.1×10-5; *p = 0.02. Results of the degranulation and cytotoxicity assays from four individual donors, performed in two pairs on two separate occasions.